

# 1 Snow Depth Estimation on Lead-less Landfast ice using Cryo2Ice

## 2 satellite observations

3 Monojit Saha<sup>1</sup>, Julienne Stroeve<sup>1,2</sup>, Dustin Isleifson<sup>1</sup>, John Yackel<sup>3</sup>, Vishnu Nandan<sup>1,3</sup>, Jack Landy<sup>4</sup>, Hoi  
4 Ming Lam<sup>3</sup>

5 <sup>1</sup>Centre for Earth Observation Science, Department of Environment and Geography, University of Manitoba, Winnipeg,  
6 Canada

7 <sup>2</sup>Department of Earth Sciences, University College London, London, United Kingdom

8 <sup>3</sup>Department of Geography, University of Calgary, Calgary, Canada

9 <sup>4</sup>Centre for Integrated Remote Sensing and Forecasting for Arctic Operations (CIRFA), UiT The Arctic University of Norway,  
10 Tromsø, Norway

11  
12 *Correspondence to:* Monojit Saha ([saham1@myumanitoba.ca](mailto:saham1@myumanitoba.ca))

13 **Abstract.** Observations of snow on ~~Arctic sea~~ Arctic Sea ice are vitally important for sea ice thickness estimation, ~~as well as~~  
14 ~~for understanding~~ bio-physical processes and human-activities. ~~While previous studies have combined CryoSat-2 and ICESat-~~  
15 ~~2-derived freeboards to estimate snow depth over Arctic sea ice, these approaches require leads within the ice pack to estimate~~  
16 ~~the freeboard heights above the sea surface. In regions such as the Canadian Arctic Archipelago (CAA), leads are scarce in~~  
17 ~~winter, posing a significant challenge to estimate snow depth from altimeters.~~ This study is the first assessment of the potential  
18 for near-coincident ICESat-2 and Cryosat-2 (Cryo2Ice) snow depth retrievals in a lead-less region of the ~~CAA including~~  
19 ~~validation with in-situ data~~ Canadian Arctic Archipelago. ~~In lieu of sea surface height estimates from leads, s~~ Snow depths are  
20 retrieved using the absolute difference in surface heights (~~ellipsoidal heights~~) from a ~~near-coincident~~ ICESat-2 and Cryosat-2  
21 after applying an ocean tide correction between satellite passes. Both the absolute mean snow depths and ~~snow depth~~  
22 distributions retrieved from Cryo2Ice were slightly underestimated (~~2 to 4 cm~~) when compared to in-situ measurements. All  
23 four in-situ sites had snow with saline basal layers and different levels of roughness/ridging ~~which significant impacts the~~  
24 ~~accuracy of the Cryo2Ice snow depth retrievals. g.~~ The retrieved Cryo2Ice snow depths were underestimated by an average of  
25 ~~33.5 % which is higher than the tidal adjustment applied (25%).~~ Differences in the Cryo2Ice and in-situ snow depth  
26 distributions reflected the different sampling resolutions between the sensors and the in-situ measurements, with Cryo2Ice  
27 missing snow depths greater than ~~340~~ cm especially around ridges. Results suggest the possibility of estimating snow depth  
28 over lead-less landfast sea ice but attributing 2-3 cm biases to differences in sampling resolution, snow salinity, density, surface  
29 roughness and/or errors in altimeter's tidal corrections require further investigation.

## 30 1 Introduction

31 Changes in Arctic sea ice are affecting climate, ecosystems and traditional ways of living and harvesting (Meier and Stroeve,  
32 2022). A critical component of the sea ice cover is its overlying snow cover, which has been challenging to accurately measure  
33 by satellites (Webster et al., 2018). Snow acts as an insulator, impacting both the growth and decay of sea ice (Maykut and  
34 Untersteiner, 1971). Snow also (1) limits the amount of light penetrating through the sea ice, affecting the timing of sea ice  
35 algae growth (Mundy et al., 2005); (2) contributes to the amount of freshwater discharged to the ocean, affecting its budget  
36 (Andersen et al., 2019); and (3) affects the heat exchange between the atmosphere and the sea ice (Andreas et al., 2005).

37 Using coincident airborne laser and radar altimeter data collected during the Laser-Radar Altimetry (LaRA) mission over sea  
38 ice around Svalbard, Leuschen et al., 2008, suggested snow depth could be retrieved by differencing freeboards, though there  
39 was a lack of in-situ ground truth to validate results. Following this, studies have differenced coincident satellite radar  
40 (CryoSat-2; hereafter CS2) and laser (ICESat-2; hereafter IS2) altimeter freeboards to estimate pan-Arctic (e.g. Kwok and  
41 Markus, 2018; Kwok et al., 2020) and Antarctic snow depth (Kacimi and Kwok, 2020). However, significant uncertainties  
42 remain related to (1) differences in electromagnetic frequencies and spatial resolution (Fons et al., 2021); (2) whether or not  
43 the CS2 Ku-band radar returns originate from the snow/ice interface, which has been contested even for a dry and cold (below  
44 freezing) snow pack (Willatt et al., 2023, 2011; Nandan et al., 2017; de Rijke Thomas et al., 2023); (3) the influence of surface  
45 roughness over different length scales on the laser and radar waveforms (Landy et al., 2019); and (4) spatial heterogeneity of  
46 snow distributed over sea ice.

47 Earlier studies also faced challenges of having different orbits for CS2 and IS2, limiting the number of ~~exact footprint~~ crossover  
48 ~~pointss~~ (Kwok & Markus, 2018). Kwok and Markus (2018) made a case for adjusting the CS2 orbit to achieve more overlaps  
49 with IS2, thereby improving both spatial and temporal coincidence. As part of the Cryo2Ice campaign, the CS2 orbit was  
50 raised by ~ 900 meters in August 2020 to significantly increase the amount of ~~IS2~~-crossovers ~~with IS2~~ (ESA, 2020). This  
51 realignment means that once in every 19 CS2 (20 IS2) cycles, the two ground tracks ~~s~~ nearly align for a few hundred kilometers  
52 over the Arctic. However, Freedensborg Hansen et al., (2024) provides the first analysis of Cryo2Ice along-track snow depths  
53 retrieved using the freeboard differencing method over 7-km segments and reports uncertainties of 10-11 cm.

54 With the Cryo2Ice campaign, new opportunities ~~have emerged are possible~~ to improve and validate snow depths retrieved by  
55 combining laser and radar freeboards. This study provides the first high-resolution in-situ validation of snow depths retrieved  
56 along coincident Cryo2Ice tracks on the 29th of April 2022 (29-04-2022) near Cambridge Bay, Nunavut in the Canadian Arctic  
57 Archipelago (CAA). The CAA is a region with significantly different bathymetry and icescape than the Central Arctic (Galley  
58 et al., 2012). Sea ice in the CAA is landfast ice for the majority of the year (6 to 8 months) (Melling, 2002), and exhibits  
59 minimal ice drift (Galley et al., 2012), ~~making it easier to match up IS2 and CS2 tracks. On the other hand, the~~ tidal amplitudes  
60 within the shallow bathymetry of the CAA are ~~also much~~ larger than in the open ocean; ~~posing an additional challenge~~  
61 ~~compared to validation stud. This poses additional challenges~~ compared to validation studies in the Central Arctic Ocean.  
62 ~~However, the~~ most prominent challenge ~~pertains to the is~~ the lack of open water for estimating the local sea surface height

(SSH) needed to reference the freeboards. Landfast ice grows along the narrow channels in the CAA and often lacks leads for several hundred kilometers (Galley et al., 2012). Therefore, assuming IS2 and CS2 are viewing the same landfast ice, the variation in SSH due to tidal variations must be known and corrected for between the two sensors. Our objective is to develop an approach to combine IS2 and CS2 along-track data in regions where the local SSH estimate is not readily available from satellite observations. The along-track Cryo2Ice retrieved snow depths are then validated using near-coincident in-situ snow depth observations. We further use in-situ snow property observations and satellite estimates of the surface roughness to examine the drivers of CS2 and IS2 height variability. Finally, the sources of bias in the retrieval process and major challenges are discussed.

## 2 Data and Methods

### 2.1 ICESat-2 (IS2)

The Advanced Topographic Laser Altimeter System (ATLAS) is the photon counting LiDAR system onboard ICESat-2. ATLAS emits low-energy 532 nm (green) pulses in three two-beam pairs which have a cross track spacing of 3.3 km between each pair with intra-pair spacing of 90 meters. The laser has a footprint size of 11 meters (Magruder et al., 2020). Detailed specifications can be found in Neumann et al., (2019).

In this study, the uncorrected ATL07 Sea Ice Height Release Version 6 available from the National Snow and Ice Data Centre (<https://nsidc.org/data/atl07ql/versions/6#anchor-2>) is used, which provides which are uncorrected sea ice heights computed directly from ATL03 photon heights are used. ATL07 contains sea surface and sea ice heights derived from heights are aggregated from ATL03 photon heights that were aggregated into segment lengths consisting of ~150 photons, resulting in variable along-track lengths over which these photos are accumulated. For this study, the ATL03 heights were aggregated over over variable distances, the heights were aggregated over 8.3 meters on average over the portion of the track used in this study to compute the ATL07 heights. In the uncorrected ATL07 product, sea ice heights within the 25 km land-buffer are included despite low confidence in the geophysical corrections close to land (Kwok et al., 2023). The IS2 strong beam (gt1) (referred to as IS2 2l) from ATL07 is used based after assessing all three strong beams on proximity to the CS2 reference ground track and field sampling sites. The IS2 2l strong beam 2l was ~1500 metre from the CS2 point of closest approach whereas the beams 1l and 3l were ~2200 metre and ~4500 metre away, respectively.

The geophysical corrections applied to the ATL07 data geophysical corrections are summarized in Table A1. Each correction is time-varying and has different impacts on the retrieved IS2 heights. The ocean tide corrections are provided every hour and can vary from -62 cm to +62 cm between -62 cm, which is the largest among the different geophysical corrections applied. The ocean tide corrections are obtained from the Global Ocean Tide Model 4.8 (GOT 4.8) (Kwok et al., 2021), which GOT 4.8 model provides tidal predictions for all regions of the globe based on the assimilation of data from satellite altimetry and tide gauge measurements into a tidal model.

94 **2.2 CryoSat-2 (CS2)**

95 The SAR Interferometric Radar Altimeter (SIRAL) is the primary instrument on board CryoSat-2, which is a combination of  
96 a pulse-limited radar altimeter along with a Synthetic Aperture Radar (SAR) Interferometer system (SARIn). SIRAL operates  
97 at Ku-band (13.575 GHz) and in three different modes with along-track sampling resolution of around 300 m and across-track  
98 resolution of 1600 m (ESA, 2013). Cryosat-2 operated in the SARIn mode in the CAA during the study period. Here we use  
99 the CS2 Level 2 Baseline E products available through the European Space Agency's EO-CAT web explorer  
100 (<https://eocat.esa.int/>). The CS2 Level 2 sea ice heights are re-tracked using the University College London (UCL) retracker  
101 (Tilling et al., 2018) which assumes a threshold (70%) on the first peak for diffuse echoes representing the mean elevation of  
102 the snow/sea ice interface within the footprint. **This fixed threshold retracker is used in the CS2 Baseline E level product over**  
103 **sea ice in the SARIn mode.**

104 Tidal corrections (ocean, long-period equilibrium, ocean loading, solid earth and geocentric polar) are included in the Level 2  
105 Baseline E Cryosat-2 SAR/SARIn product (Table B2). The ocean tide, long-period equilibrium tide and ocean loading tide  
106 corrections used are retrieved from the Finite Element Solution 2004 Ocean Tide Model (FES 2004) (Cryosat-2 Product  
107 Handbook). The ocean tide corrections typically range from  $\pm 50$  cm.

108 **2.3 Field Measurements**

109 The study site comprised a 75 km long NNE-to-SSW transect across Dease Strait (69°26'58.02"N 106°41'57.25"W to  
110 68°46'42.48"N 106°55'52.10"W) (Figure 1), ~70 km west of Cambridge Bay, NU. This region connects Coronation Gulf and  
111 Queen Maud Gulf of the Kitikmeot Sea and is a part of the southern route of the Northwest Passage (Xu et al., 2021). Dease  
112 Strait is relatively shallow (maximum depth ~ 100 meters), and its narrow channel is covered by landfast ice normally between  
113 November and mid-July (Galley et al., 2012). CS2 and IS2 coincident tracks were identified using the CS2 and IS2 Coincident  
114 Data Explorer (<https://cs2eo.org/>) (Ewart et al., 2022). The tracks were ~1.5 km apart and passing by within 77 minutes of  
115 each other (Figure 1).

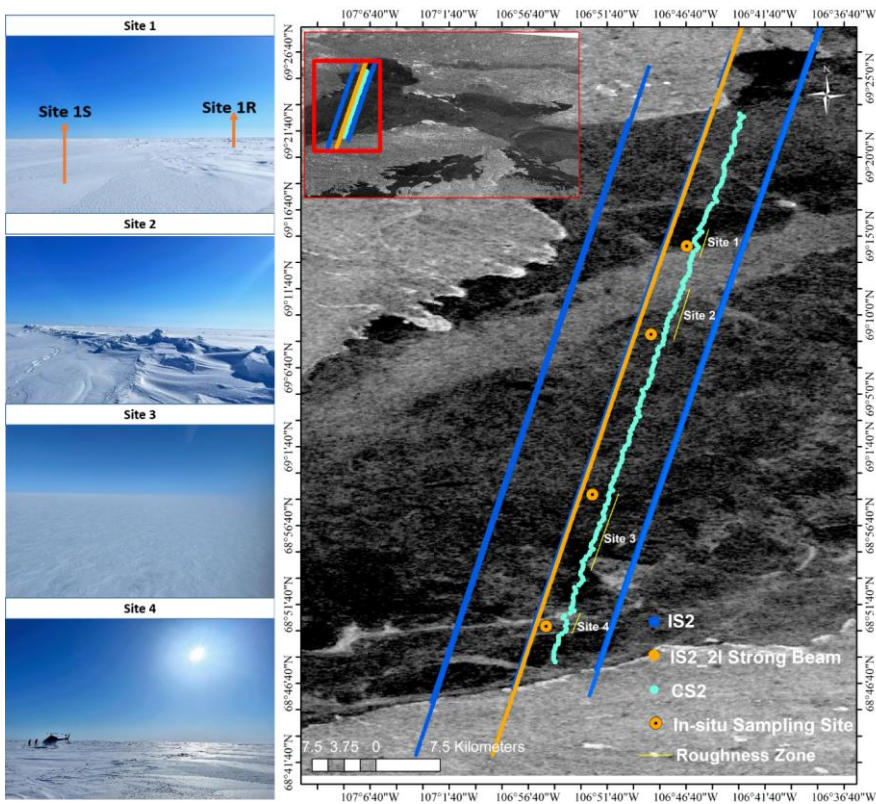


Figure 1 Map shows the Cryosat-2 Points of Closest Approach (POCA) locations, IS2 2l Strong Beam and other IS2 beam, in-situ sampling locations and identified roughness zones. The background contains Sentinel-1 HH-pol SAR imagery. Site photos show the variation in snow roughness.

In-situ snow depths were collected at four different sites (Sites 1-4) ranging from smooth, rough and mixed sea ice roughness zones. The transects were set considering wind direction as well as the sea ice surface features for each site. The sampling strategy was to ensure coverage of the Cryo2Ice along-track and across-track directions, taking into consideration the prevailing wind direction and different representative roughness features. At Site 1, two L-shaped transects representing the rough and smooth sea ice zones were conducted (Figure D1 (a)). For Site 2, two different L-shaped transects were conducted to sample both the ridged ice areas zone as well as the smoother ice zones further away from the ridges were both covered (Figure D1(b)). For Sites 3 and 4 which had wider regions of smooth and rough sea ice respectively, two L-shaped transects were conducted (Figure D1 (c) & (d)). Based on Sentinel-1 SAR and field reconnaissance, Site 1 was classified as a rough and

128 smooth sea ice transition zone; Site 2 was a thin snow zone with significant ridging; Site 3 was a smooth sea ice zone with  
129 extensive areas of thin snow; and Site 4 was a rough sea ice site with extensive areas of thick snow. All sites were located  
130 equidistant between the IS2 strong beam and CS2 track to ensure the highest likelihood that snow depth sampling was  
131 representative of both sensors. The snow depth sampling direction was determined according to distinctive roughness features  
132 at individual sites, ensuring sufficient sampling distance in both the along- and across-track directions, representative of the  
133 prevailing east-southeast wind direction (ECCC, 2022) and snow dune pattern (Moon et al., 2019). Snow depth was surveyed  
134 using Snow-Hydro's automated snow depth magnaprobe, which has an accuracy of  $\pm 0.3$  cm on level sea ice and snow (Strum  
135 and Holmgren, 2018). The magnaprobe was reassembled and re-calibrated before each sampling effort to avoid instrument  
136 bias. Sampling was conducted by a single person to avoid variations in instrument handling and to maintain constant intervals  
137 between samples.

138 All four sites were surveyed on 01-05-2022 within 48 hours of the ICESat-2 and CryoSat-2 pass on 29-04-2022. The sites  
139 were accessed via helicopter and no sampling was conducted within 200 meters of the helicopter landing zone to avoid snow  
140 redistribution during landing. ~~While t~~The sampling interval was initially set at 5 m intervals to ensure spatial  
141 heterogeneity and to avoid spatial autocorrelation of the sampled snow depth values following (Iacozza and Barber, (1999).  
142 However, the sampling interval ranged between ended up was higher (2 to 3.8 metre ) during the field sampling for all sites.  
143 There ~~was~~ no precipitation recorded during the sampling period, nor during the time interval between the CS2 and IS2  
144 overpasses. Furthermore, high pressure dominated the region between 26-04-2022 and 04-05-2022 causing light surface winds.  
145 As such, snow redistribution between CS2 and IS2 overpasses and in-situ sampling was negligible. The air temperature varied  
146 between  $-11.7^{\circ}\text{C}$  and  $-14.1^{\circ}\text{C}$  during the sampling as measured at the Cambridge Bay, land-based meteorological station.  
147 Snow geophysical properties including snow salinity and density were sampled from all four sites. Snow temperature was not  
148 measured because the temperature probe would not calibrate quickly enough between the short helicopter landing durations.  
149 For Site 1, two pits were sampled, one for the rough sea ice (Site 1a) and one for the relatively smooth sea ice zone (Site 1b).  
150 Single pits were excavated at the other three sites. Snow density was measured using a  $66\text{ cm}^3$  ( $2 \times 5.5 \times 6$  cm) density cutter  
151 at 2 cm intervals and weighed in the lab. ~~After, w~~weighed samples were then-melted at room temperature for snow salinity  
152 measurement using a Cole-Parmer C100 Conductivity Meter (accuracy of  $\pm 0.5\%$ ). Sea ice thickness and freeboard at each  
153 site was measured using a freeboard tape to an accuracy of 0.5 cm.

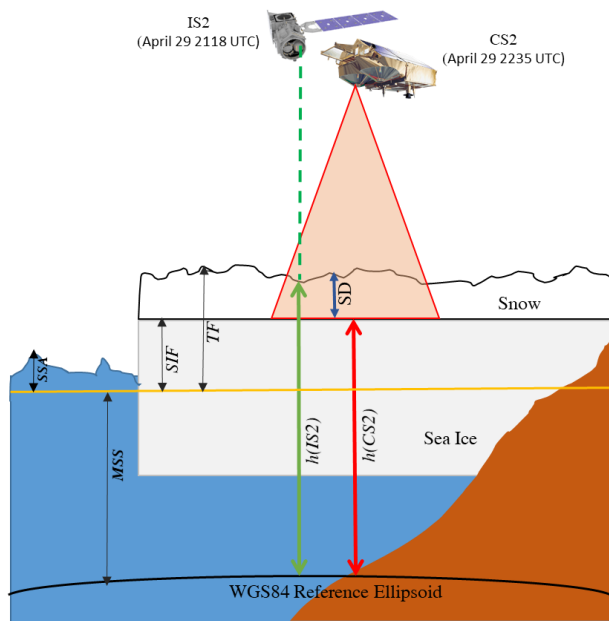
#### 154 2.4 Estimating Snow Depth from Cryosat-2 and ICESat-2

155 Kwok et al (2020) calculates snow depth (SD) as the difference between IS2-derived total freeboard (snow + ice) and-CS2-  
156 derived ~~sea ice radar~~ freeboard (CS2). ~~Freeboard heights are computed relative to the , using the difference between the surface~~  
157 ~~height and the~~-instantaneous sea surface height interpolated from sea surface measurements from along-track leads to (Kwok  
158 et al., 2020; Ricker et al., 2014). ~~The CS2 radar freeboard is additionally~~also adjusted for reduced Ku-band propagation speed  
159 through snow to derive an accurate estimate of the sea ice freeboard. While this approach has been applied to the Cryo2Ice  
160 ~~campaign within the central Arctic (Fosberg et al., 2024), freeboards require~~ ~~However, reliable freeboard measurements from~~

161 ~~IS2 and CS2 are dependent on~~ accurate estimation of the sea surface height which is dependent on the availability of leads  
162 within a reasonable distance (10's of km) along both the IS2 and CS2 track. No leads were detected along the portion of the  
163 IS2 and CS2 tracks in ~~our~~ the study area and therefore the sea surface height could not be ~~reliably~~ -estimated. Therefore, we  
164 modified the approach used in Kwok et al., (2020) ~~to instead use the~~ ~~We used the~~ absolute sea ice heights measured from IS2  
165 ATL07 (h(IS2)) and CS2 (h(CS2)) referenced to the WGS84 ellipsoid to estimate SD (Figure 3). SD can be calculated as the  
166 freeboard differences under the assumption that Ku-band penetrates to the snow/ice interface

$$167 \quad SD = \frac{h_{IS2} - h_{CS2}}{\eta_s}, \quad (1)$$

168 Where  $\eta_s$  is the refractive index of Ku-band microwaves which compensates for the propagation delay through the snow pack  
169 (Kwok et al., 2020). The refractive index is calculated using  $(\eta_s = (1 + 0.51\rho_s))^{1.5}$  (Ulaby et al., 1986), where the in-situ bulk  
170 snow density ( $\rho_s$ ) measured from the field is used. The average snow density from all four sites is used to compute snow depth  
171 for the entire track (Figure 8) while snow densities from each site are used to compute SD from corresponding portions of the  
172 Cryo2Ice track (Figure 5).



173  
 174 **Figure 2** Schematic showing the calculation of snow depth (SD) from ICESat-2 and Cryosat-2 over sea ice. The diagram illustrates  
 175 the representative heights for the sea surface anomaly (SSA), mean sea surface (MSS) in yellow, sea ice freeboard (SIF) and total  
 176 freeboard (TF). SD is shown with the blue arrow, IS2 surface height ( $h(IS2)$ ) is shown with the green arrow and CS2 surface height  
 177 ( $h(CS2)$ ) is represented by the red arrow. Land is orange.

## 178 2.5 Data Processing

179 ~~Both the IS2 ATL07 and CS2 heights are referenced to the WGS84 ellipsoid (Figure 2).~~

180 The uncorrected IS2 ATL07 heights ( $h(IS2)$ ) are referenced to the WGS84 ellipsoid which is also consistent with the CS2  
 181 heights (Figure 2). In our processing of the ATL07 data we apply the following geophysical corrections which are contained  
 182 within the IS2 ATL07 product: ocean tide correction, long-period equilibrium tide and inverted barometer correction. We do  
 183 not apply the mean sea surface (MSS) ~~since it~~ since it is based on decadal averages and therefore is not representative of the  
 184 variation of sea surface heights within the 77 minute -1 hour interval between the IS2 and CS2 passes. The geophysical  
 185 corrections included within the CS2 data product are applied to the CS2 L2 sea ice heights. However, as mentioned previously  
 186 the two products do not have the same tidal corrections. ~~The tides varied ~6.0 cm in Dease Strait in between the two passes,~~  
 187 ~~based on the two sets of tidal corrections, requiring an ocean tide correction factor to be derived to account for the variation in~~  
 188 ~~absolute SSH between the IS2 and CS2 acquisitions (Section 2.6).~~



189 Further, there is limited confidence in these individual geophysical corrections closer to land. ~~Moreover, The~~ tides varied  
190 over a range of ~ 6.0 cm in Dease Strait in between the two passes, so it was crucial to check if the tidal corrections contained  
191 within the products accurately accounted for tide differences in the ~77 minutes between passes. Therefore, after comparing  
192 the geophysical correction as explained in Section 2.6, an ocean tide correction factor is applied to the Cryo2Ice snow depths.  
193 Since IS2 has a smaller footprint (Section 2.1 and 2.2), the IS2 ATL07 geolocated heights were averaged to be spatially  
194 congruent with the CS2 footprint giving snow depths estimates in the maximum along-track resolution of 300 m. Here, the  
195 IS2 photons are first averaged over 300 m length segments to match the along-track CS2 footprint and then co-registered based  
196 on the distance to the closest CS2 Point of Closest approach. Similarly, to reduce the impact of CS2 noise as explained later  
197 in Section 4.3, the snow depths are also computed over 1-km. Therefore, each CS2 point is co-registered to the closest 300  
198 metre ATL07 height segment. Snow depths computed from the IS2 and CS2 height differences were estimated following  
199 Equation (1), and subsequently adjusted with the ocean tidal correction. To identify the extent of spatial heterogeneity in the  
200 retrieved snow depths from Cryo2Ice, the Moran's I test (Moran, 1948) is performed to test the level of spatial autocorrelation.  
201 The semi variogram analysis of the in-situ snow distribution shows that the snow depth values are correlated within a lag  
202 distance of ~1 kilometer. Therefore, to compare snow distributions representative of each sampled field site (S1 to S4), snow  
203 depth is compared over similar roughness zones. Roughness zones corresponding to each Site are defined as a portion of the  
204 CS2/IS2 track which had IS2 surface roughness within one standard deviation of the IS2 derived surface roughness directly  
205 adjacent to the in-situ sampling site (Figure 1). The Cryo2Ice-derived snow depth corresponding to each roughness site was  
206 then compared against the in-situ snow distribution from the sampling sites.

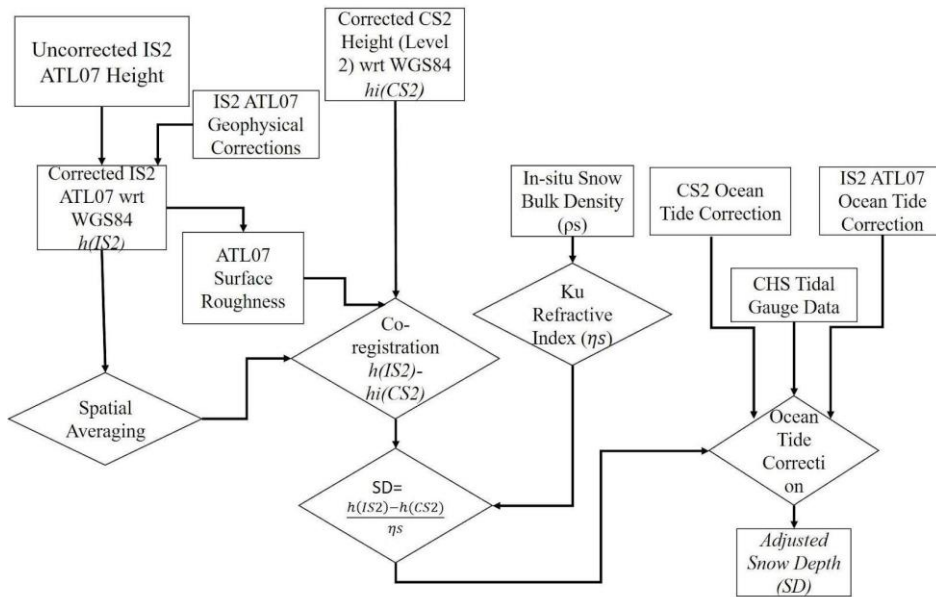


Figure 3 Methodological workflow for retrieving snow depth (SD) from CS2/IS2 co-registered averaged ATL07 ( $h(IS2)$ ) and Cryosat-2 heights ( $h(CS2)$ ) are subtracted following Equation 1. The differenced product is located at the Point of Closest Approach (POCA) of each CS2 footprint. The differenced product is then adjusted with the refractive index ( $\eta_s$ ).

## 2.6 Adjusting for Sea Surface Height Variation

Assuming IS2 and CS2 are viewing the same landfast ice, any variation in sea surface height over the short 77 minute interval between tracks is assumed to be due to tidal variations. The long-period equilibrium tide and ocean-tide with the inverted barometer corrections were compared between the sensors to identify differences between them. As mentioned earlier, different ocean tide corrections are applied to CS2 and IS2, with values ranging between +/-50 cm in CS2 and +/-62 cm in IS2 (Kwok et al, 2021, Cryosat-2 Product Handbook), and these have the most significant impact on the height retrievals (Figure C1, See Figure S1 in Bagnardi et al., 2021). Ideally, the ocean tide correction applied to IS2 and CS2 should account for the true variation in SSH due to local tides between the data acquisition passes. Although sea ice significantly dampens tides (Rotermund et al., 2021), tidal fluctuations, in this case the tidal corrections were found to be non-negligible. We compared the average ocean tide corrections to local tidal gauge predictions from the Canadian Hydrographic Service (CHS) (<https://tides.gc.ca>) which are based on real-time and historical tidal gauge measurements from the Cambridge Bay station. The CHS dataset provides instantaneous tidal variations at the CB station every 15 minutes with six observations between the IS2 and CS2 passes. The difference in ocean tidal corrections between the IS2 and CS2 pass was 7.9 cm on average along the

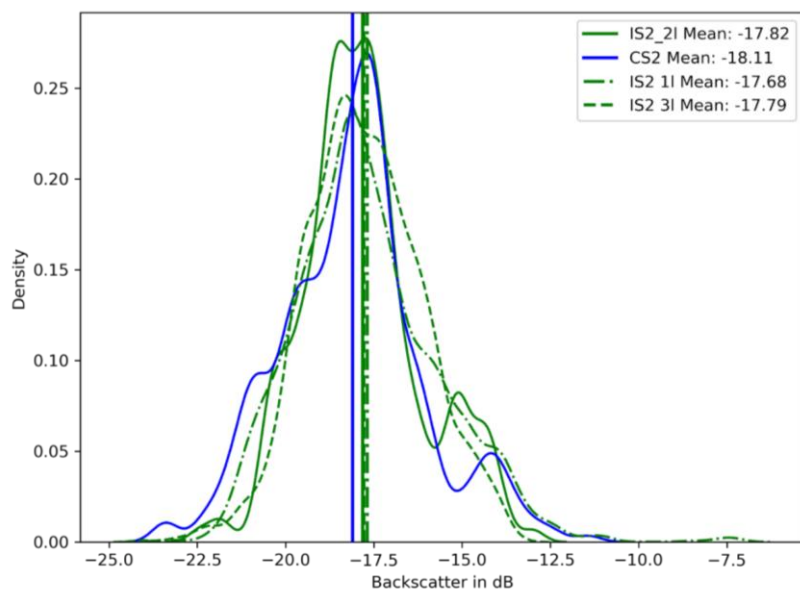
224 track whereas the difference in water level was 6.0 cm according to the CHS data. The difference in height between IS2 and  
225 CS2 was therefore adjusted by a single value of 1.9 cm before the snow depths were computed (Figure 3) and this value then  
226 represents a systematic uncertainty on the final snow depth estimates.

## 227 **2.7 Evaluating Other Sources of Uncertainties**

228 One of the critical assumptions is that IS2 and CS2 tracks are roughly coincident i.e. both tracks are measuring roughly the  
229 same snow despite their reference ground tracks being ~1.5 km apart. ~~In order to~~ test this assumption, Sentinel-1 backscatter  
230 (which roughly indicates the snow distribution; Cafarella et al., 2019) was characterized across both the IS2 and CS2 reference  
231 ground tracks. ~~Given that IS2 has three different strong beams (IS2 11,21 and 31), we compare the SAR backscatter across all~~  
232 ~~three tracks and compare it to the SAR backscatter along the CS2 track. We notice that along the IS2 21 track the SAR~~  
233 ~~backscatter shows the most similar backscatter distribution as along the CS2 track (Figure 4). This also aligned with~~  
234 ~~the fact that the IS2 21 beam was the closest (~1.5 km) from the CS2 Points of Closest Approach (POCA) and therefore would~~  
235 ~~see the most similar snow distributions. Therefore, the strong beam IS2 21 was considered for the subsequent Cryo2Ice~~  
236 ~~snow depth calculations.~~ The SAR pixels intersecting with the IS2 and CS2 track were used to calculate the mean backscatter  
237 along each track. The mean difference in SAR backscatter was -0.3 dB, ~~less~~ less than 1 standard deviation of the  
238 backscatter of each track (Figure 4). Since both the tracks have similar backscatter, the assumption that they are coincident  
239 and observing snow packs with the same distribution is likely valid. ~~Additionally, the difference in the point-to-point~~  
240 ~~point-to-point~~ backscatter between IS2 and CS2 was also calculated to assess whether the difference in backscatter is consistent  
241 throughout the track (Figure G1). We see that the average difference in backscatter between the collocated points is within -  
242 +1 dB. The average difference in backscatter between IS2 and CS2 is 0.9 dB. Since both the tracks have similar backscatter,  
243 the assumption that they are coincident and observing snowpacks with the same distribution is likely to be valid.

244

245



246 **Figure 4 Sentinel-1 Backscatter in dB** obtained from all the strong beams of IS2 (IS2 1I, 2I and 3I) and CS2 track locations. The  
 247 Sentinel-1 VH backscatter from 05-05-2022 is used for extracting backscatter along both the tracks to assess whether the observed  
 248 snow distribution is similar.  
 249

250 Landy et al (2019, 2020) demonstrated the importance of considering surface roughness in the radar data processing. Sea ice  
 251 surface roughness was computed across the IS2 track using the ATL07 sea ice height product. Surface roughness was  
 252 calculated as the standard deviation of ATL07 sea ice height product following Farrell et al., (2020). However, instead of the  
 253 25 km distance set for pan-Arctic studies, the regional differences in surface roughness were calculated over 300-meter length  
 254 segments to maintain consistency with the spatially averaged ATL07 heights.

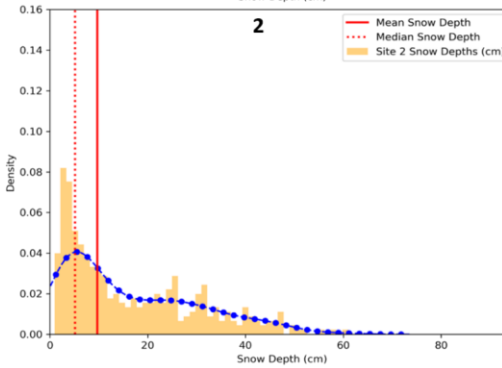
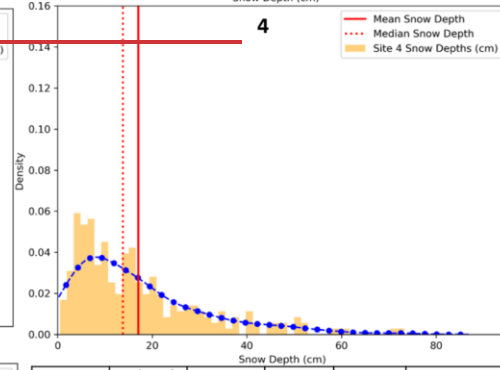
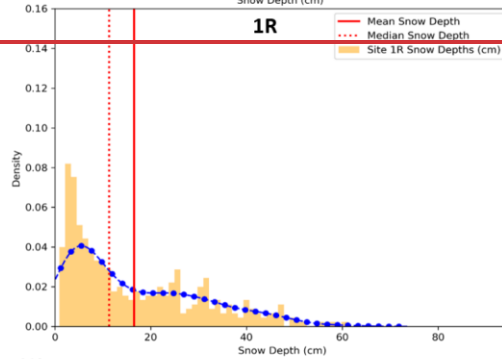
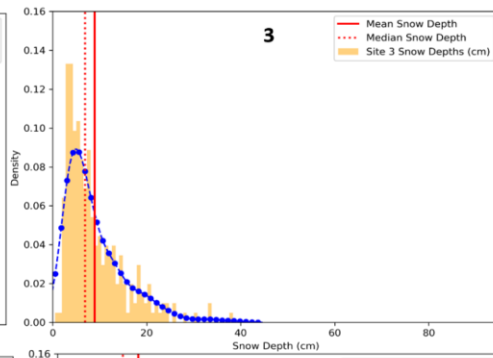
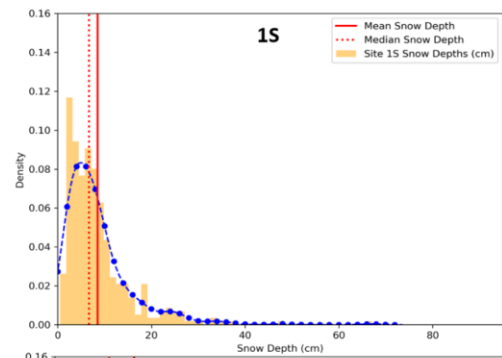
255 Previous studies measured or modelled the dominant scattering surface over first-year sea ice (FYI) at Ku-band (Nandan et  
 256 al., 2017, 2020; Willatt et al., 2011)– several to many centimeters above the snow/sea ice interface even for cold snowpacks.  
 257 Nandan et al. (2017, 2020) argue that when brine is present within the snowpack, the dominant scattering horizon at Ku-band  
 258 is shifted upwards by approximately 7 cm above the snow/sea ice interface. Mallett et al., (2020) further demonstrated that the  
 259 use of fixed snow densities introduced significant biases in the snow depth retrievals. Provided snow salinity impacts the  
 260 location of the Ku-band dominant scattering horizon (Nandan et al., 2017), an assessment was conducted to test the bias  
 261 introduced by choosing different snow bulk densities by (a) assuming Ku- band microwaves penetrate completely through the  
 262 snow layers to the sea ice surface and (b) Ku-band microwaves penetrates through layers with snow salinity less than 1 ppt.

263 The corresponding average in-situ snow bulk densities from (a) the complete snow layer (b) snow layers with less than salinity  
264 of 1 ppt were used to compute refractive indices followed by respective snow depth calculations. There was negligible  
265 difference in the refractive index ( $<0.05$ ) considering the snow bulk densities with difference in salinity and therefore the  
266 average bulk densities from the complete snow pack was used in this study.

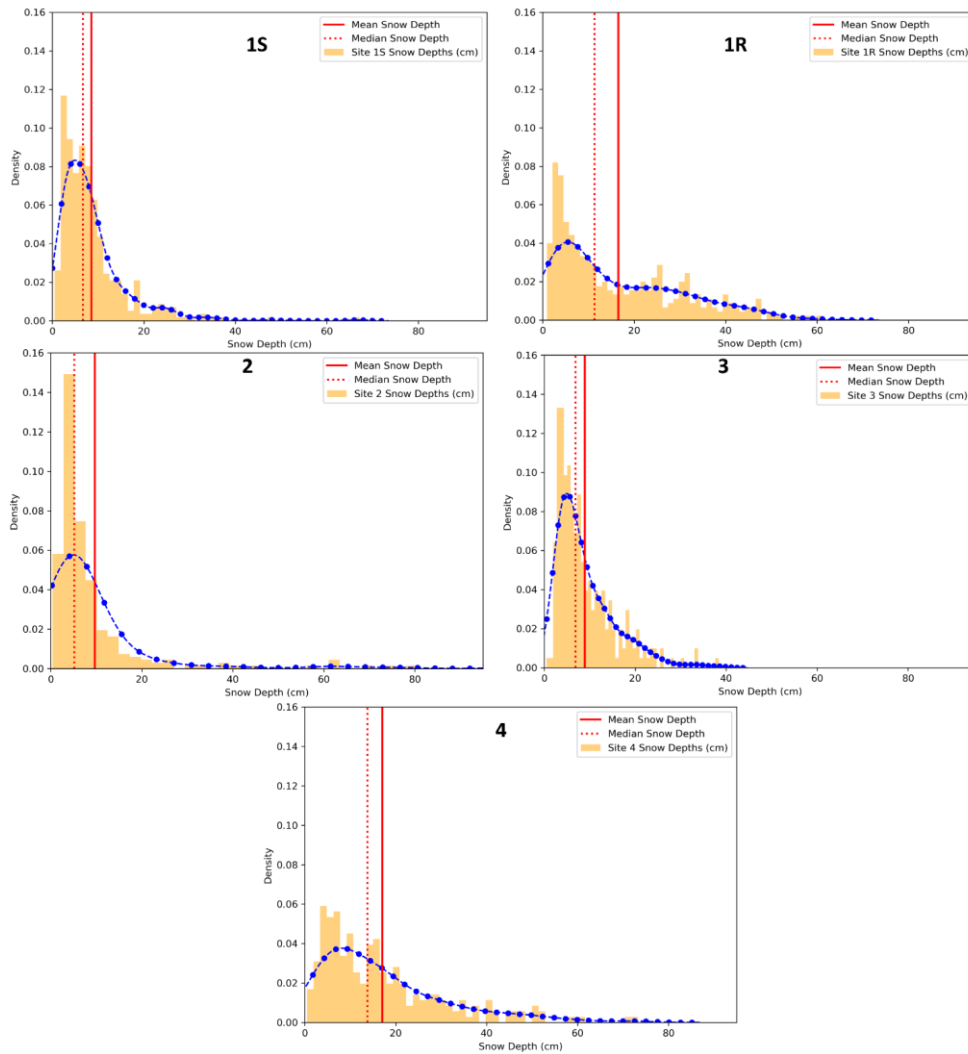
### 267 3. Results

#### 268 3.1 In-Situ Snow Depths and Distributions

269 In-situ snow depths demonstrate significant spatial variability among the four sampled sites (Figure 5). The mean snow depth  
270 from the four different sites varies between 9 and 17 cm, and all sites have positively skewed distributions (Figure 5). Site 2  
271 also has some exceptionally high snow depths ( $> 90$  cm), corresponding to the ridged areas (Figure 5) and therefore show  
272 higher standard deviations (Figure 5). Sites 2 and 3 have similar snow distributions (Figure 5) but the presence of ridging in  
273 Site 2 results in a wider tail compared to Site 3. The maximum snow depth of 80 cm was recorded in Site 2 which was picked  
274 up directly adjacent to the ridge. Site 4 has the highest mean snow depth (Figure 5) as well as the thickest tailed snow  
275 distribution (Figure 5). The distinctive snow depth characteristics were also evident from the standard deviation of snow depth  
276 among the four sites. Site 2 which had significant ridging also had the highest standard deviation of snow depth (15.8 cm).  
277 Site 1R and Site 4 which had rougher sea ice both had high standard deviations of snow depth (13.7 (Site 1R) and 13.9 (Site  
278 4)).



Site Number	Number of Samples	Distance Sampled (m)	Mean Snow Depth (cm)	Min/Max Snow Depth (cm)	Standard Deviation (cm)
1S	431	862	8.51	0.5 / 7.3	7.2
1R	376	752	16.5	0.9/61.01	13.7
2	276	1240	9.7	0.5 / 80	15.8
3	268	930	8.9	0.5 / 38.4	6.4
4	244	850	17.1	0.5 / 73.3	13.9



280

281

282

**Figure 5** Snow depth distributions from the four in-situ field measurement sites along the Cryo2Ice transect. **The table presents descriptive statistics for the snow depth measurements. The density distribution curve is shown in blue.**

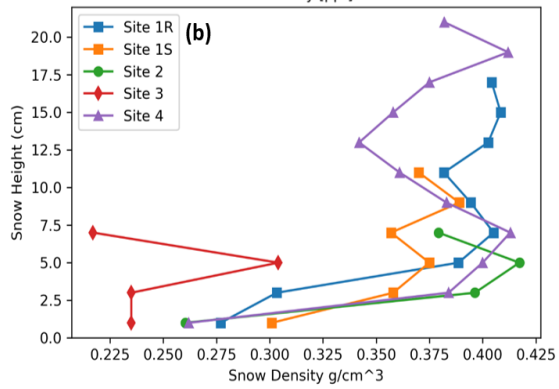
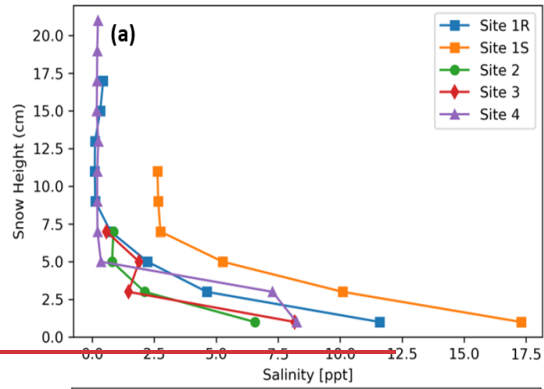
283 **3.2 Snow Geophysical Parameters**

284 Mean snow salinity varies between 1.5 to 3.0 ppt for Sites 1S, 2, 3 and 4, whereas at Site 1S the snow salinity is 6.78 ppt  
285 (Figure 6). The mean snow bulk density varies between 0.358 and 0.374 g/cm<sup>3</sup> in all sites except Site 3 where the mean snow  
286 density is 0.248 g/cm<sup>3</sup>.

287 Vertical profiles of snow salinity and bulk density present further insights. As shown in Figure 6.7, the snow density patterns  
288 are similar for Sites 1R, 1S, 2 and 4 with bulk density ranging between 0.260 to 0.420 g/cm<sup>3</sup> and lower at the base of the  
289 snowpack than the surface (Figure 6). The snow density varies in the different snow layers but there is a general trend towards  
290 higher densities at 4 to 7 cm above the snow-ice interface at all sites (Figure 6). This is attributed to the presence of a wind  
291 slab snow layer most prominent at Sites 1R, 2 and 4.

292 Snow salinity shows higher salinities closer to the snow-ice interface but decreasing with height up the interface (Figure 6 (a)).  
293 For snow pits greater than 7.5 cm thick, the salinity is less than 1 ppt closer to the air-snow interface. There is a spike in salinity  
294 between 5 to 3 cm from the snow-ice interface at Site 3 that corresponds to the high bulk density snow layer (Figure 6(b)).





Sites	Mean Salinity (ppt)	Mean Bulk Density (g/cm <sup>3</sup> )
Site 1R	2.25	0.374
Site 1S	6.78	0.358
Site 2	2.58	0.363
Site 3	3.02	0.248
Site 4	1.59	0.370

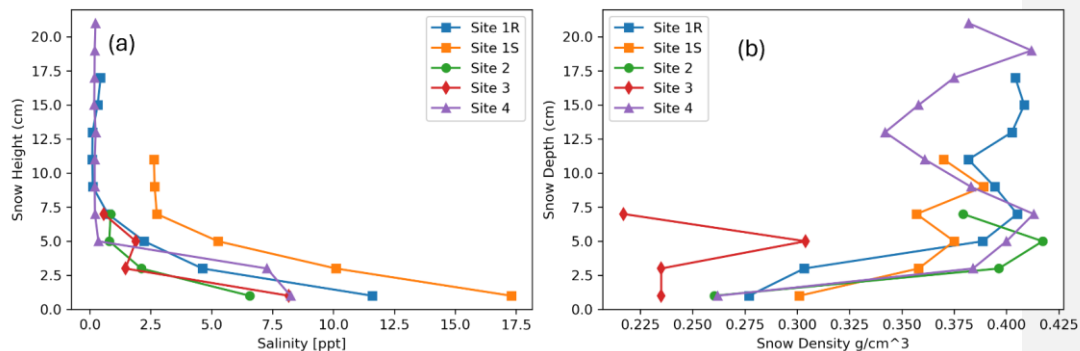
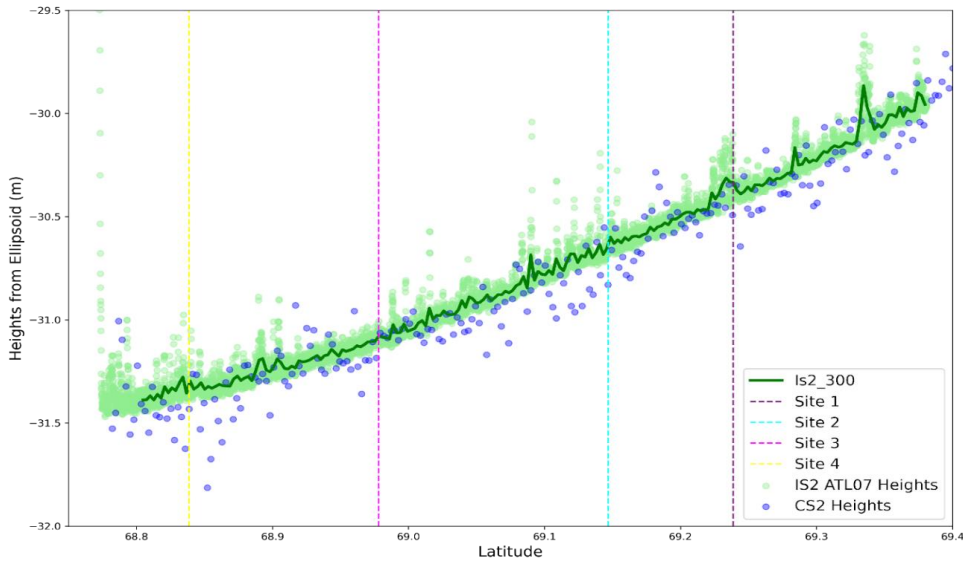


Figure 6 (a) Snow salinity and (b) Snow density change by snow pack depth at the four snow sampling sites. Zero snow depth in both plots represents the snow-ice interface. The bottom table shows the variation in mean salinity and bulk density among the different sites.

### 3.3 ICESat-2/Cryosat-2 Derived Snow Depths

Snow depths were calculated based on the ellipsoidal height difference between the IS2 2I and CS2 after adjusting for the difference in tides as explained in Section 2.6 (Figure E1). IS2 2I was closest to the CS2 Points of Closest Approach (POCA) which ensured that the uncertainty due to the difference in spatial collocation of IS2 and CS2 was minimized as explained in Section 2.7. The CS2 ( $h(CS2)$ ) and IS2 ( $h(IS2)$ ) heights show a general pattern of lower CS2 heights in comparison relative to co-registered IS2 heights (Figure 7). The correlation of the CS2 ellipsoidal height with the Cryo2Ice snow depth (0.2509) is higher than the IS2 ellipsoidal heights (-0.1213) which shows implies that the snow depths would be impacted more by the noise in CS2 heights compared to IS2. The  $h(IS2)-h(CS2)$  differences range between -26.5 cm and 50.0 cm with a mean difference of 7.9 cm. The difference 20% of the calculated differences are negative which and the negative snow depth points are distributed randomly along the track (Figure 8). While negative snow depths don't have a physical basis, we include them in the subsequent snow depth calculations so as to not discard the impacts of altimeter noise on the retrieved heights (Fredensborg Hansen et al., 2024). However, the noise in the CS2 heights as evident in Figure 7, corresponds with the large negative snow depth values (Figure 7, Figure 8). Therefore, to reduce the negative bias in snow depths due to the CS2 noise, we exclude negative snow depth values which are two standard deviations away from the mean Cryo2Ice snow depths in the subsequent calculations (Figure 9).

The adjusted mean snow depth across the whole Cryo2Ice track is 7.4 cm, which is lower than the mean snow depth of 11.9 cm retrieved from the four in-situ sites surveyed (Figure 5). A maximum snow depth of 39.4 cm is retrieved from Cryo2Ice, at a length scale of 300 m which is significantly lower than the maximum snow depths measured in situ > 90 cm.

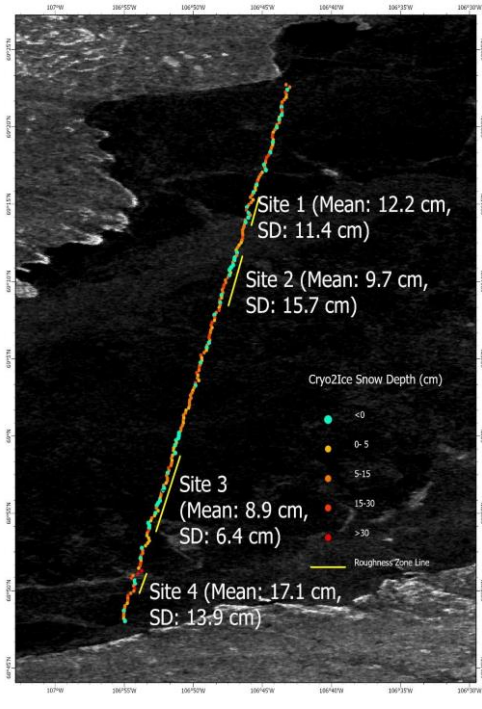


319

320 **Figure 7 IS2 ATL07 sea ice heights plotted along with CS2 surface heights. Note, the reported heights are relative heights and can**  
 321 **be negative because of the WGS84 ellipsoid reference heights in the study area. The light green color indicates the raw ATL07**  
 322 **heights (IS2 ATL07 Heights). The solid green line indicates the aggregated ATL07 heights aggregated every 300 meters (IS2\_300).**  
 323 **The purple color indicates the CS2 Heights.**

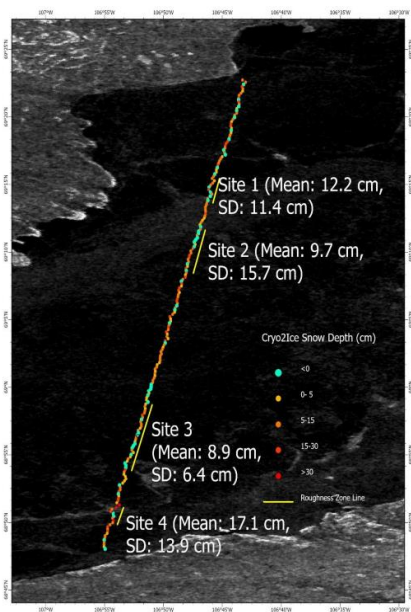
324 Snow depths shown in Figure 9 display a right-skewed distribution with a sharper and heavier tail compared to a normal  
 325 distribution. This is consistent with the distributions obtained from the in-situ snow sites (Figure 5). Analyzing the spatial  
 326 distribution of the retrieved snow depths demonstrates that there is high spatial variability in the retrieved Cryo2Ice snow  
 327 depths. The semivariogram analysis indicates that there is spatial autocorrelation among measured snow depths within ~1  
 328 km but there is no significant autocorrelation for larger distances, along this specific track-. This also implies that there is significant  
 329 spatial heterogeneity above the km-scale along the ~65 km track (Figure 8). The snow depths are correlated at scales under ~1

330 km which correspond with the lengths of the representative portions of the track delineated with similar roughness (Figure 8).

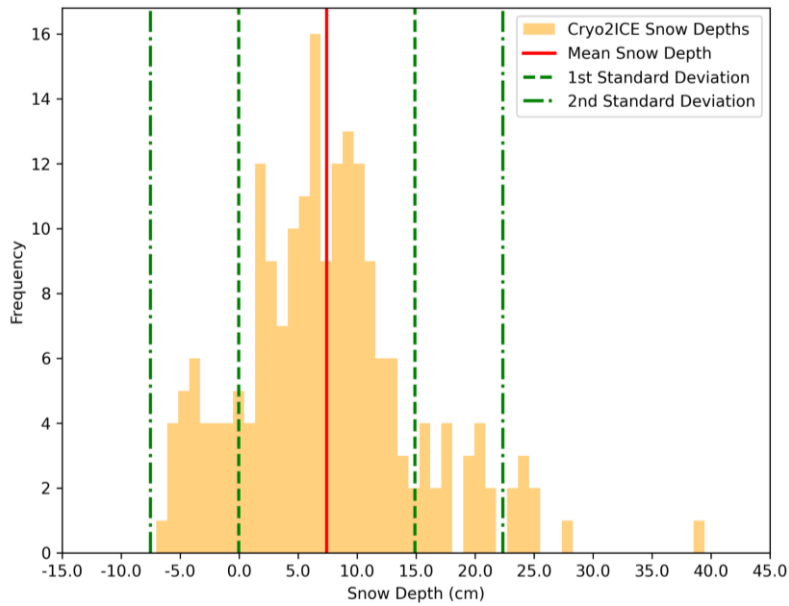


331  
332 Figure 8 Spatial distribution of 300-m scale Cryo2Ice snow depths across the CS2 and IS2 derived track. The background image is  
333 a Sentinel-1 HH backscatter image from 5-05-2022. The mean and standard deviation (SD) of the in-situ snow depths are labelled  
334 for surveyed sites included inside brackets.

335



336  
 337 **Figure 8 Spatial distribution of 300-m scale Cryo2Ice snow depths across the CS2 and IS2 derived track. The background image is**  
 338 **a Sentinel-1 HH backscatter image from 5-05-2022. The mean and standard deviation (SD) of the in-situ snow depths are labelled**  
 339 **for surveyed sites included inside brackets.**



340

341 **Figure 9** Histogram showing the density distribution of the retrieved snow depth in the native 300 m resolution along the Cryo2Ice  
 342 track with the mean and the median snow depths. Negative snow depths greater than 2 standard deviations from the mean snow  
 343 depth were removed to reduce the impact of CS2 noise.

344 **4 Discussion**

345 **4.1 Comparison with Past Studies**

346 Previous field observations from Yackel et al. (2019) and Nandan et al. (2020) suggest that mean snow depth on FYI in Dease  
 347 Strait during late winter ranges between 10 and 30 cm depth (Table 1). While our mean in-stu snow depth measurements (11.9  
 348 cm) is within the typical range reported in previous surveys, we see that the Cryo2Ice mean snow depth (7.44 cm–)  
 349 underestimated the observed snow depths (Table 1).

350

351

352 **Table 1** In-situ snow depth measurements at Dease Strait. The range of mean snow depths represents the range of mean snow depths  
 353 retrieved from the sampled sites.

354

Sampling Period	Mean Snow Depth (cm)	Number of Sites Sampled	Total Number of Samples	Sampling Technique	Reference
20 April to 9 June, 2014	13.5	24	24	Snow Pits	Campbell et al., (2016)
12 May to 17 June, 2014	20.8	2	60	Meter Rule Sampling	Diaz et al., (2014)
19-22 April, 2014	12.0/18.0	20	5200	Meter Rule Sampling	Zheng et al., (2017)
23-26 May, 2016	12.0/22.0	4	2100	Meter Rule Sampling	Moon et al., (2019)
01-08 April, 2017	17.0/ 35.0	5	2161	Magnaprobe Sampling	Moon et al., (2019)
17-19 May, 2018	20.9 / 21.8	3		Magnaprobe Sampling	Yackel et al., (2019)
1 May, 2022	11.9	4	1596	Magnaprobe Sampling	This Study
Cryo2Ice Snow Depths	7.44 (Mean), 39.4(Maximum)				

355

356 **4.2 Snow Depth: Cryo2Ice vs In-situ**

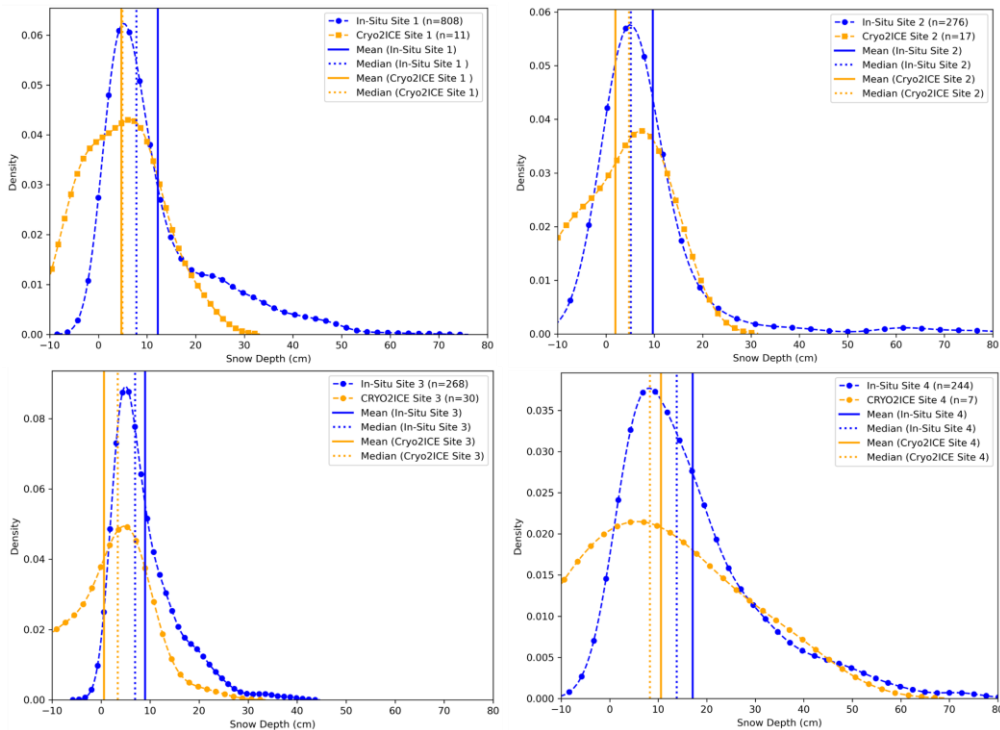
357 Cryo2Ice snow depths showed similar relative patterns when compared to in-situ snow depth sampling. The thinnest (Site 3)  
 358 and thickest (Site 4) mean snow depths found in the in-situ measurements are corroborated with Cryo2Ice snow depths as well.  
 359 The Kruskal-Wallis non-parametric test was conducted to assess statistically significant differences between the snow depths

360 retrieved from the in-situ and Cryo2Ice. The test results show significant difference between in-situ sites which was also  
361 evident in the corresponding Cryo2Ice snow depths.

~~362 Given the positively skewed distributions retrieved from both in situ and Cryo2Ice, the median bias was considered for  
363 evaluating the satellite retrieved snow depths. Considering the median bias of snow depths reduces the impact of the outliers  
364 i.e. the retrieved negative snow depths as well. Cryo2Ice snow depths are on average 3.07 cm thinner than the in-situ data,  
365 which is a 1 cm larger difference than the manual tidal correction we applied to compare the CS2 and IS2 track heights (i.e.,  
366 the largest known systematic uncertainty during processing) (Figure F1). This pattern of a few cm mean snow depth  
367 underestimations by Cryo2Ice is consistently observed across four sites (Figure 10)(Table F1). The median bias (<1 cm) is  
368 lowest in Site 2 where the median snow depth from Cryo2Ice. However, in Site 2 which was the significantly ridged site, the  
369 snow depths greater than 30 cm which are adjacent to the ridge are largely missed by Cryo2Ice (Figure 10). The largest median  
370 bias was recorded in Site 4 which was the roughest sea ice zone also having the thickest snow. However, Snow depths greater  
371 than 30 cm were relatively better picked up by Cryo2Ice (Figure 10). These mismatches may be caused by the difference in  
372 sampling length scales between Cryo2Ice, which is at the kilometer scale, compared to in situ measurements which are  
373 retrieved over 100s of meters. It is evident that while IS2 has a much finer resolution, the larger footprint of CS2 means that  
374 the spatial variability of snow depths under the kilometer scale are not well represented by Cryo2Ice. For instance, the Cryo2Ice  
375 snow depths are consistently truncated at the thick end of the distribution, with at least some portion of the in-situ distributions  
376 above ~30-50 cm seemingly unresolved from space (Figure 10).~~

~~377 In terms of the overall shape of the distributions, the best match is found for Site 3 which has the lowest median snow depth  
378 among the sites. Therefore, we see that Cryo2Ice generally performs better in smoother sea ice zones when compared to  
379 rougher sea ice zones such as Site 1, 2 and 4. We notice that site with the highest standard deviation of snow depths retrieved  
380 from in situ transects i.e. Site 4 seemed to have the highest median snow depth bias (5 cm). Therefore, we see that although  
381 some of snow depths greater than 30 cm seem to be better represented at Site 4, the overall retrieved snow depth distribution  
382 is underestimated. We also notice that the Cryo2Ice snow depth distributions are generally wider than the in-situ distributions  
383 which is due to the impact of the higher negative snow depths significant negative snow depths which are included in the  
384 calculation. These negative snow depths, while included in the initial calculations to reflect the true native resolution results,  
385 don't have a physical basis, leading to artificial widening of the distributions in Figure 10.~~





387  
388 **Figure 10** Probability Density plots comparing In-Situ snow depths to Cryo2Ice retrieved snow depths along with the median and  
389 mean values. Different snow bulk densities were used to calculate the refractive index and subsequently Cryo2Ice snow depths for  
390 each site (Site 1-0.399 g/cm<sup>3</sup>, Site 2- 0.398 g/cm<sup>3</sup>, Site 3- 0.217 g/cm<sup>3</sup>, Site 4-0.381 g/cm<sup>3</sup>). The detailed statistics for the  
391 comparison are provided in Table F1.

392 **4.3 Adjusting for the Difference in CS2 and IS2 Footprint**

393 As noted in Section 4.2, the difference in CS2 and IS2 footprint size with IS2 having a significantly smaller footprint compared  
394 to CS2 leads to a significant underestimation of the retrieved snow depths in the native 300 m resolution. Therefore, to reduce  
395 the impact of this artificial underestimation of the distribution, we average both IS2 and CS2 over a larger along-track distance.  
396 While averaging the CS2 and IS2 over 1-km causes some of the prominent roughness features such as ridges to be missed by  
397 Cryo2Ice, the snow depths from the 1-km CS2 and IS2 averaged heights are more realistic representations of the snow  
398 distributions when compared to in-situ (Figure 11). The average snow depth from the 1-km averaged CS2 and IS2 heights  
399 represents the overall shapes of the in-situ snow depths better compared to the native 300-meter averaged heights (Figure 11).  
400 The shapes of the distributions are well represented especially in Site 1 and 2. We also notice that shapes of the Cryo2Ice snow  
401 depth distributions match best in Site 1 and 2 compared to in-situ. However, the general underestimation of snow depths is  
402 reflected within most of the Sites (Site 1, 2, 3) except Site 4 which seems to overestimate the snow depth (Figure F2). The  
403 average snow depth retrieved from the 1-km averaged product is 7.80 cm which is slightly higher than the 300-meter averaged

Formatted: Font color: Red

Formatted: Font color: Red

Formatted: Font color: Red

product presented in Section 3.3. The median bias between the in-situ and the 100 km averaged product is less than 2 cm in Sites 1 and 2. (Figure 11) (Tabel F2).

Comparing the shapes of the distributions, we see that almost all the sites have similar snow depth distributions compared to in-situ sites (Figure 11). However, a significant portion of the tails of the distributions are still missing which was also evident in the 300 m snow depth product. While the shapes of the distributions in Sites 3 and 4 are similar compared to in-situ, the peaks of the distribution don't coincide well. Cryo2Ice snow depths in Site 1 has the most similar distribution to in-situ compared to the other sites. In Site 2 we also see very similar snow depth distributions between Cryo2Ice and in-situ even between the 20 to 30 cm snow depths. While the shapes of the distributions match well in Site 3, we see a shift towards negative snow depths indicating that negative snow depths caused by noise in CS2 has larger impacts here in the smoother sea ice. Cryo2Ice seems to perform worst in Site 4 which is the roughest sea ice zone, with Cryo2Ice snow depths being overestimated when compared to in-situ. This is also evident in the shapes of the 1-km adjusted snow depth product which seems to be skewed towards higher snow depth values (Figure 11). Therefore, after adjusting for the difference in footprint size and averaging over 1-km along-track distance, the overall snow depth distributions are more similar to in-situ for the majority of the sites.

Formatted: Font color: Red

Formatted: Font color: Red

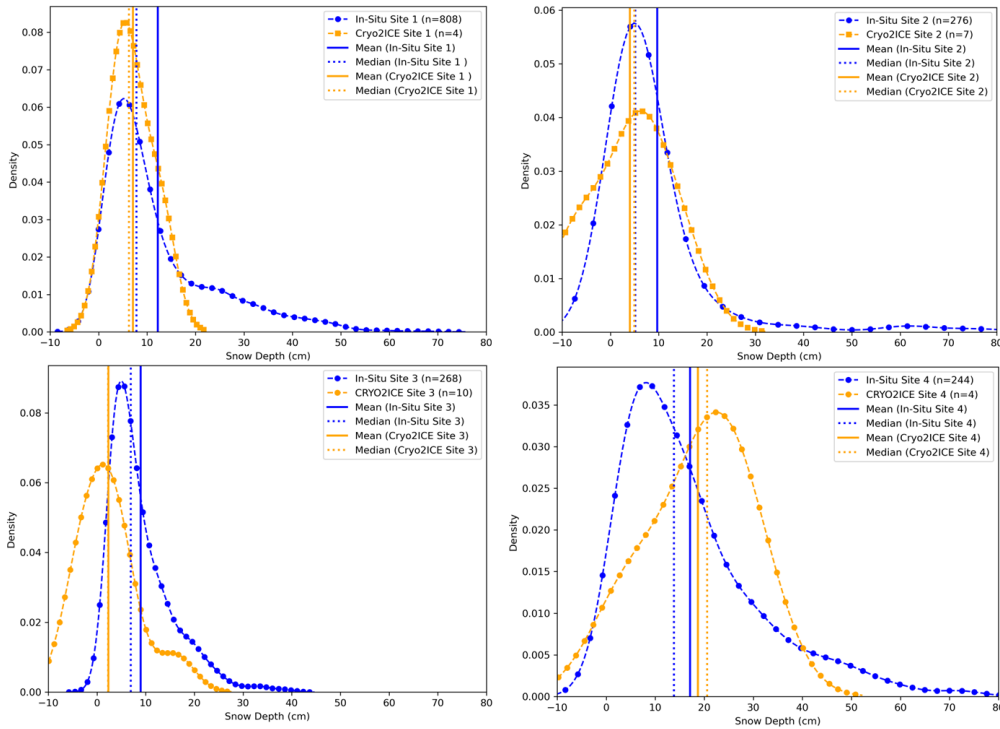


Figure 11 Probability Density plots comparing In-Situ snow depths to Cryo2Ice retrieved snow depths retrieved from 1-km averaged CS2 and IS2 heights along with the median and mean snow depth values. Different snow bulk densities were used to calculate the

421 refractive index and subsequently Cryo2Ice snow depths for each site (Site 1-0.399 g/cm<sup>3</sup>, Site 2- 0.398 g/cm<sup>3</sup>, Site 3- 0.217  
422 g/cm<sup>3</sup>, Site 4-0.381 g/cm<sup>3</sup>). The detailed statistics for the comparison are provided in Table F2

#### 424 4.3 CS2 Noise Adjusted CryoIce Snow Depths

425 Snow depths retrieved in the 300 meter resolution presented in Section 3.3 include the negative snow depths within two  
426 standard deviations of the mean snow depths. We attribute this phenomena to the noise in CS2 heights which are reflected by  
427 the wide fluctuations in the heights compared to the IS2 heights (Figure 7). Such noise in CS2 ultimately leads to significant  
428 negative Cryo2Ice snow depths (20%). These negative snow depths, while included in the initial calculations in order to reflect  
429 the true native resolution results, don't have a physical basis, leading to negative bias leading to artificial widening of the  
430 distributions in Figure 10. Therefore, in order to reduce the impact of CS2 noise, we test the impact of averaging both CS2 and  
431 IS2 over 1 km lengths before comparing to the in-situ snow depth and distributions. We see that averaging the CS2 over 1 km  
432 significantly reduces the impact of CS2 noise in the snow depth retrievals. While averaging the CS2 and IS2 over 1 km causes  
433 some of the prominent roughness features such as ridges to be missed by Cryo2Ice, the snow depths from the 1 km CS2 and  
434 IS2 averaged heights are more realistic representations of the snow distributions when compared to in-situ (Figure 11). The  
435 average snow depth from the 1 km averaged CS2 and IS2 heights represents the overall shapes of the in-situ snow depths  
436 better compared to the native 300 meter averaged heights (Figure 11). The shapes of the distributions are well represented  
437 especially in Site 1 and 2. We also notice that shapes of the Cryo2Ice snow depth distributions match best in Site 1 and 2  
438 compared to in-situ. However, the general underestimation of snow depths is reflected within the majority of the Sites (Site 1,  
439 2, 3) with the exception of Site 4 which seems to overestimate the snow depth (Figure F2). The average snow depth retrieved  
440 from the 1 km averaged product is 7.8 cm which is slightly higher than the 300 meter averaged product presented in Section  
441 3.3. The median bias between the in-situ and the 100 km averaged product is less than 2 cm in Sites 1 and 2. Therefore, we  
442 demonstrate that using a length scale of 1 km significantly reduces the noise in CS2 heights and therefore leads to a better  
443 representation of the snow depth distributions compared to in-situ. However, it must be mentioned that there is significant loss  
444 of detailed sea ice features such as ridges due to the averaging of features which were better represented in the native 300-  
445 meter resolution (Figure 8).

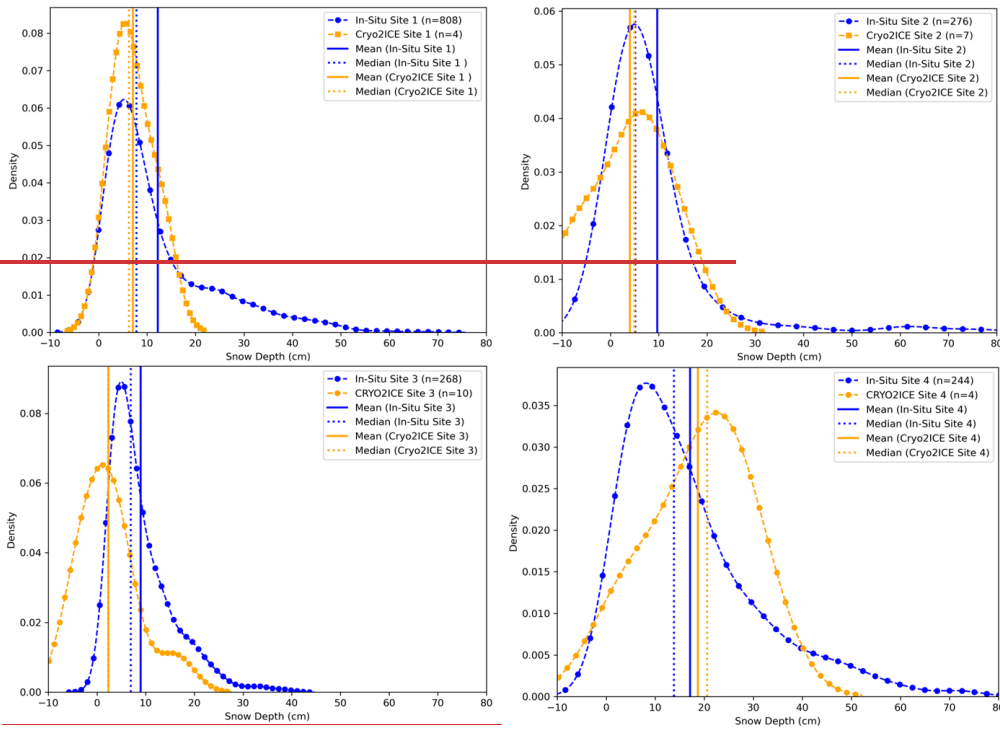


Figure 11 Probability Density plots comparing In-Situ snow depths to Cryo2Ice retrieved snow depths retrieved from 1-km averaged CS2 and IS2 heights along with the median and mean snow depth values. Different snow bulk densities were used to calculate the refractive index and subsequently Cryo2Ice snow depths for each site (Site 1  $0.399 \text{ g/cm}^3$ , Site 2  $0.398 \text{ g/cm}^3$ , Site 3  $0.217 \text{ g/cm}^3$ , Site 4  $0.381 \text{ g/cm}^3$ ). The detailed statistics for the comparison are provided in Table F2

#### 4.4 Snow Geophysical Properties and Cryo2Ice Retrievals

Both snow salinity and bulk density changes across the snowpack layer impacts the IS2 laser and CS2 radar waveform interactions with the snowpack. While the IS2 green laser is mostly impacted by the air-snow interface conditions, CS2 radar waveforms interact with different layers of the snowpack and the dominant scattering horizon and subsequently radar heights can potentially be impacted by the snow properties. There were significant differences among the snow salinity and density characteristics (Figure 6) between the surveyed sites. However, we notice that higher snow depths i.e. greater than 30 cm were picked up better in Site 4 which also had the lowest mean salinity with 17 cm out of the 22 cm deep snowpack being non-

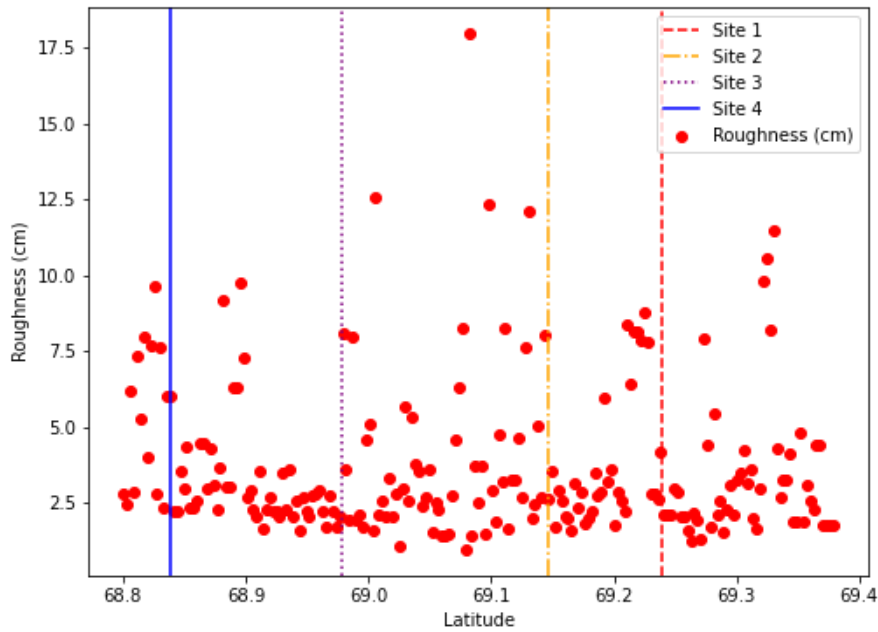
459 saline. Therefore, the maximum intensity of the CS2 backscatter may have been sourced from closer to the sea-ice interface in  
460 Site 4. On the contrary, highly saline layers can potentially raise the height of dominant scattering intensity of the Ku-band  
461 radar leading to overestimated CS2 heights ( $h(CS2)$ ) and subsequently lower mean snow depth compared to in-situ values.  
462 This phenomenon of snow depth underestimation was evident in Sites 1R, 1S, and 2 potentially because of the sharp  
463 increase in snow salinity within the first 5 cm (from the air-snow interface) of the snowpack (Figure 6) and may have  
464 contributed to ~2 the 2-3 cm underestimation of Cryo2Ice snow depths. ~~We notice that Cryo2Ice shows median bias of 2.88~~  
465 ~~cm in Site 1 where snow pit 1S had a significantly higher salinity across the snowpack which may be behind the~~  
466 ~~underestimation compared to in-situ (Figure 6)~~  
467 The impact of snow bulk density on the Cryo2Ice retrievals was less likely except for the presence of wind-slab layers which  
468 are identified as stark increases in snow bulk densities within the snowpack. ~~The wind-slab layers were identified in~~  
469 ~~Site 1R in Sites 1R and 4 where the density reached to reach to 0.425 g/cm<sup>3</sup> compared to 0.358 to 0.374 g/cm<sup>3</sup> on average~~  
470 ~~throughout the snowpack which which may have caused hindrance to Ku-band penetration which may have contributed to~~  
471 ~~median underestimations.~~ The presence of this high-density snow layer along with the reduction in Ku-band speed due to  
472 power attenuation of Ku-band microwaves may potentially cause a cumulative upward shift of the dominant scattering horizon  
473 resulting in underestimation of snow depths. However, it is difficult to ascertain such uncertainties to a single physical factor  
474 due to interdependency of the processes.

#### 475 4.5 Sea Surface Height Estimation and Cryo2Ice Retrievals

476 Canadian Hydrographic Service (CHS) tidal predictions for 29 April 2022 suggest the satellite overpasses occurred during a  
477 low tide period. According to the predictions, the water level was 6 cm higher for the IS2 pass at 21:18 UTC than for the CS2  
478 pass at 22:35 UTC (Figure C1). This 6 cm water level difference should ideally be accounted for by the difference in IS2 and  
479 CS2 ocean tide corrections. The IS2 ATL07 heights were reduced by a mean ocean tide correction of -0.71 cm whereas the  
480 CS2 Heights reduced by an average ocean tide correction of -8.64 cm. Therefore, the difference between IS2 heights and CS2  
481 heights was increased by 7.9 cm due to the ocean tide correction adjustment but the CHS predictions suggest it should have  
482 been only 6.0 cm. ~~This 1.9 cm difference would introduce a 25.5 % bias in retrieved snow depths, given the approx. mean~~  
483 ~~snow depths we measured in-situ.~~ This error could be attributed to the ocean tide corrections used in IS2 and CS2 originating  
484 from two different models i.e. GOT 4.8 (IS2) and FES 2004 (CS2). To put this source of error into wider context, past CS2  
485 and IS2 coincident tracks from 15-04-2021 and 14-05-2021 were also analysed. We found a bias of 2 to 5 cm when compared  
486 with the CHS dataset, meaning that we can expect ~15-40% systematic uncertainty in Cryo2Ice retrieved snow depths owing  
487 to the uncertainty in tidal differences between satellite passes. This is a significant uncertainty, but it is systematic and varies  
488 at the length-scale of the tidal corrections (100s km), so it will not affect the *relative* variations in retrieved snow depth along  
489 track, only their *absolute* magnitude. Therefore, Cryo2Ice seems capable of measuring the relative variations in snow depth  
490 between different locations of the CAA without the availability of sea surface reference tie-points.

#### 4.6 Surface Roughness and Cryo2Ice retrievals

Surface roughness calculated from IS2 was used to analyze the Cryo2Ice snow depths between sites with different roughness. There was only a weak positive correlation ( $R^2$  0.04) between surface roughness retrieved from IS2 and Cryo2Ice snow depths. Site 4 had the highest mean surface roughness (4.58 cm) whereas the other sites had roughness ranging between 2.4-2.7 cm. Although there was significant ridging in Site 2 and IS2 does pick up some of the ridges (Figure 7), the mean surface roughness is low (2.48 cm) because of the extensive areas of thin snow cover which dominates the laser returns. While Site 4 had the highest snow depth as well as highest surface roughness from IS2 which also corresponds with the, the Cryo2Ice retrievals at Site 4 had the highest median bias (Figure 4-Table F20). Therefore, we notice that Cryo2Ice performs poorly in regions with relatively high surface roughness. However, one stark difference was the fact that there was no ridging in Site 4. Therefore, while there were extensive areas of rough sea ice with snow depths between 20 and 50 cm which are generally well represented by Cryo2Ice, there were hardly any snow depths greater than 80 cm unlike Site 2 (Figure 10). We also notice that for Site 2, most of the snow was very thin with only a few very high snow depth points especially around the ridges (Figure 10). The presence of isolated ridges and the deeper snow accumulated around them may have been missed by the CryoSat-2 radar given the larger impact of level ice versus ridges on the backscattered power which may explain the underestimation in Sites 1 and 2. The ridge heights may also be underestimated with current ICESat-2 processing methods (Ricker et al., 2023) meaning that snow depths would be underestimated. The higher variability which is indicated by the standard deviation of snow depths translates to greater median bias in snow depth (Figure 5).



509 **Figure 12.4** Variation in surface roughness along the Cryo2Ice track at the four in-situ snow thickness validation sites

512 **5 Conclusion**

513 Accurate snow depth monitoring over landfast ice in the Canadian Arctic Archipelago (CAA) is important for communities  
 514 that rely on landfast ice for transportation and their livelihood (Mahoney et al., 2009). It is imperative to monitor snow depth  
 515 in the CAA as there have been reports of declining snow depths at a rate of 0.8 cm per decade in Cambridge Bay and at other  
 516 locations in the CAA (Howell et al., 2016; Lam et al., 2023). Moreover, the ~~y~~-reported snow depth on sea ice trends were  
 517 highly correlated to the declining sea ice thickness. Therefore, this study explores the potential of retrieving snow depth using  
 518 Cryo2Ice in a lead-less regions of the Canadian Arctic Archipelago. ~~While previous studies (Freesborgen Hansen et al., (2024)~~  
 519 ~~have compared snow depths over larger segments (7 km) and used snow depth products from passive microwave, snow models~~  
 520 ~~or climatologies, this study is the first comparison of Cryo2ice snow depths to in-situ snow depth retrievals over ~~300-meter~~300-~~  
 521 ~~meter and segments1-kilo meter segments.~~

522 Snow depth from Cryo2Ice is retrieved based on the elevation difference between IS2 and CS2 sea ice heights from a common  
523 ellipsoid as opposed to the popular freeboard differencing method. The instantaneous difference in sea level between the 77  
524 minute ~1.5hour difference between the CS2 and IS2 passes is accounted for by adjusting the ocean tide corrections with local  
525 tide model predictions. The snow depths retrieved from Cryo2Ice compare favourably with in-situ snow depth measurements  
526 when averaged over 1-km segments of the tracks. The relative snow depth patterns from in-situ field sites were corroborated  
527 with Cryo2Ice measurements, i.e. the thinnest and thickest snow depth regions were picked up correctly by Cryo2Ice. The 300  
528 meter averaged Cryo2Ice snow depths shows an average of The mean snow depth from Cryo2Ice of 7.44 cm which is slightly  
529 underestimated when compared to in-situ measurements from this study (11) and previous studies conducted at the Dease  
530 Strait. While the ~2 to 3 cm underestimation demonstrates that Cryo2Ice can estimate snow depth with reasonable accuracy  
531 after adjusting for the tidal uncertainty (Freesborgsen Hansen et al., (2024) reports uncertainties of 10-11 cm uncertainties),  
532 there are still significant sources of both systematic and random uncertainties that need to be addressed. We note that median  
533 biases ranging from 2 to 5.5 cm are reported among the different Sites which is often higher than the tidal correction applied  
534 (1.9 cm). We note that uncertainties ranging between 15-40% may be caused due to bias in tidal corrections applied between  
535 IS2 and CS2 which is larger than random uncertainties caused by noise in CS2, surface roughness and snow geophysical  
536 properties.

537 The site-wise comparison between in-situ snow depths and Cryo2Ice snow depths show that Cryo2Ice performs well in regions  
538 with moderately thin and smooth snow on sea ice i.e. ranging between 5 to 20 cm while it struggles to pick up snow depths  
539 greater than 30-50-cm irrespective of the roughness characteristics. This phenomenon is largely attributed to the difference in  
540 footprint size between CS2 and IS2 where the large footprint of CS2 missed a lot of the high snow depth sites particularly the  
541 ones close to the ridges which are otherwise picked up by IS2. Differences in the shapes of the distributions from in-situ sites  
542 and representative roughness zones of the Cryo2Ice are mostly a result of the difference in sampling resolutions of Cryo2Ice  
543 (~300 m) and the in-situ measurements (5 m). The tails of the in-situ snow depth distributions (> 40 cm) were largely missed  
544 by Cryo2Ice and the Cryo2Ice snow depth retrieval accuracy is impacted by the presence of sea ice ridges. We also notice that  
545 negative snow depths mostly retrieved from rougher sea ice zones spatially coincides with the noisy CS2 heights which are  
546 significantly higher than the IS2 heights. These negative snow depths (20 % of the Cryo2Ice estimates) significantly skew the  
547 snow depth distributions retrieved. We note that the number of negative freeboards (20%) is much larger than the 3% negative  
548 snow depths reported in Fredensborg Hansen et al., (2024)- which we believe is mostly due to the fact that this study considers  
549 a single track as opposed to the region scale in the aforementioned study which is considered a much larger region compared  
550 to our single track. Therefore, we see that the noisy nature of CS2 data especially- especially in the rough-landfast ice plays a  
551 major factor in the underestimation of the snow depths retrieved from Cryo2Ice. Differences in the shapes of the distributions  
552 from in-situ sites and representative roughness zones of the Cryo2Ice are mostly a result of the difference in sampling  
553 resolutions of Cryo2Ice (~300 m) and the in-situ measurements (5 m). The tails of the in-situ snow depth distributions (> 40  
554 cm) were largely missed by Cryo2Ice and the Cryo2Ice snow depth retrieval accuracy is impacted by the presence of sea ice  
555 ridges. This impact leads to an artificial widening of the snow depth distributions which are obtained in the native 300-meter



556 resolution. After adjusting for this difference by averaging both IS2 and CS2 heights over 1-km instead, more realistic snow  
557 depth distributions are obtained. We note that while Cryo2Ice generally underestimates snow depths by 2 to 4 cm compared  
558 to in-situ, the 1-km averaged snow depths also show the possibility of overestimation. Therefore, we see that the impact of  
559 noisy CS2 data may be much higher on snow depths retrieved over land-fast ice.

560 Snow geophysical properties, especially snow salinity in the deepest few centimeters of the snowpack, may impact the  
561 dominant scattering center of the CS2 radar return and can lead to underestimation of the snow depths. The 1-km averaged  
562 snow depth was slightly underestimated three out of in-all-four sites compared to in-situ measurements however the median  
563 biases compared to in-situ are less than 5 cm. However, Median Cryo2Ice snow depths—reducing the impact of the missing  
564 thick snow tail in Cryo2Ice snow depth distributions shows bias less than 5 cm compared to in-situ field estimates. This study  
565 identifies several different sources of uncertainty such as noise in the CS2 heights, tidal corrections, surface roughness and  
566 snow geophysical properties which significantly impact the snow depth retrievals in addition to the uncertainty due to the tidal  
567 correction. However, it is difficult to determine given the centimeter level few centimeters of bias to snow geophysical process,  
568 surface roughness and/or errors in the altimeters' tidal corrections given that a lot of these uncertainties are inter-related and  
569 are highly variable among different length scales. Therefore, a further comprehensive study across different regions  
570 is required to isolate the impacts of these uncertainties and determine their contributions to the total uncertainty. Additionally,  
571 there are uncertainties such as the use of a fixed threshold retracker in CS2 which is not tuned for the landfast sea ice and  
572 uncertainties associated with the IS2 fine tracker that may also contribute significantly to the snow depth retrievals. Therefore,  
573 further studies are required in different lead-less regions under varying snow conditions for improved insights into the sources  
574 of bias in snow depth retrievals from Cryo2Ice. It is also noteworthy that the suggested method of using ellipsoidal heights  
575 from IS2 and CS2 with the tidal correction may also be applied in regions beyond the landfast sea ice in the Canadian Arctic  
576 Archipelago (CAA). However, as the current method relies on using tidal gauge station data from a nearby station, this method  
577 may not be directly applicable for regions that don't have a tidal gauge station nearby. However, tidal predictions from tide  
578 models that consider the impact of sea ice on the tidal amplitude such as Nucleus for European Modelling of the Ocean  
579 (NEMO) may be used instead to estimate the difference in tides between the passes. While this study suggests the use of  
580 Ellipsoidal heights for landfast ice, the freeboard differencing approach as suggested in Kwok et al., (2020) is better suited for  
581 regions where getting a direct estimation of the sea surface height and direct estimates of the freeboard are available. Findings  
582 from this study are encouraging for estimating snow depth on land-fast sea ice in lead-less regions using Cryo2Ice and for  
583 future coincident laser-radar or dual-frequency altimeter missions.

#### 584 **Data Availability**

585 ICESat-2 ATL07 data may be accessed from the NSIDC website (See: <https://nsidc.org/data/atl07ql/versions/6#anchor-2>).

586 Cryosat-2 data may be accessed from ESA (<https://eocat.esa.int/>). The snow depth validation dataset is available from the

587 CanWin Data Hub [https://canwin-datahub.ad.umanitoba.ca/data/dataset/cambridge\\_bay\\_snowdepth\\_apr2022](https://canwin-datahub.ad.umanitoba.ca/data/dataset/cambridge_bay_snowdepth_apr2022).

588

589 **Author Contribution**

590 MS, JS and DI were involved in the conceptualization of the study. MS, JS, JY, HML and VN were involved in planning of  
591 the field campaign. JS acquired the funding for the research. MS, JY and HML collected the snow and sea ice physical property  
592 validation data from the field. MS, JS, DI, JL and VN were involved in formulating the methodology for the analysis. MS  
593 prepared the original draft. All co-authors were involved in the review and editing process.

594 **Competing Interests**

595 At least one of the (co-)authors is a member of the editorial board of The Cryosphere.

596 **Acknowledgements**

597 The authors would like to acknowledge Torsten Geldsetzer from the University of Calgary for his input during the planning  
598 stages of the Cambridge Bay campaign. We acknowledge Nathan Kurtz from NASA for providing early ICESat-2 ATL07  
599 release 006 data which was vital for the analysis. MS was supported by ArcticNet (Grant Number #52551), Julienne Stroeve's  
600 NSERC Canada 150 Chair (Grant Number #50297), and John Yackel's NSERC Discovery Grant (RGPIN-2017-04888) and  
601 University of Manitoba Graduate Student Fellowship (UMGF). We also acknowledge support from ArcticNet Field Aircraft  
602 Support for the helicopter support.  
603

604 **References**

- 605 Andersen, O. B., Nilsen, K., Sørensen, L. S., Skourup, H., Andersen, N. H., Nagler, T., Wuite, J., Kouraev, A., Zakharova, E.,  
606 and Fernandez, D.: Arctic freshwater fluxes from earth observation data: International Review Workshop on Satellite Altimetry  
607 Cal/Val Activities and Applications, Fiducial Reference Measurements for Altimetry, 97–103,  
608 [https://doi.org/10.1007/1345\\_2019\\_75](https://doi.org/10.1007/1345_2019_75), 2019.
- 609 Andreas, E. L., Jordan, R. E., and Makshtas, A. P.: Parameterizing turbulent exchange over sea ice: the ice station weddell  
610 results, *Boundary-Layer Meteorology*, 114, 439–460, <https://doi.org/10.1007/s10546-004-1414-7>, 2005.
- 611 Bagnardi, M., Kurtz, N. T., Petty, A. A., and Kwok, R.: Sea Surface Height Anomalies of the Arctic Ocean From ICESat-2:  
612 A First Examination and Comparisons With CryoSat-2, *Geophys. Res. Lett.*, 48, e2021GL093155,  
613 <https://doi.org/10.1029/2021GL093155>, 2021.
- 614 Beaven, S. G., Lockhart, G. L., Gogineni, S. P., Hossetnmostafa, A. R., Jezek, K., Gow, A. J., Perovich, D. K., Fung, A. K.,  
615 And Tjuatja, S.: Laboratory measurements of radar backscatter from bare and snow-covered saline ice sheets, *International  
616 Journal of Remote Sensing*, 16, 851–876, <https://doi.org/10.1080/01431169508954448>, 1995.

617 Blanchard-Wrigglesworth, E., Webster, M. A., Farrell, S. L., and Bitz, C. M.: Reconstruction of Snow on Arctic Sea Ice,  
618 *Journal of Geophysical Research: Oceans*, 123, 3588–3602, <https://doi.org/10.1002/2017JC013364>, 2018.

619 Brunt, K. M., Neumann, T. A., and Smith, B. E.: Assessment of ICESat-2 Ice Sheet Surface Heights, Based on Comparisons  
620 Over the Interior of the Antarctic Ice Sheet, *Geophysical Research Letters*, 46, 13072–13078,  
621 <https://doi.org/10.1029/2019GL084886>, 2019.

622 Cafarella, S. M., Scharien, R., Geldsetzer, T., Howell, S., Haas, C., Segal, R., and Nasonova, S.: Estimation of Level and  
623 Deformed First-Year Sea Ice Surface Roughness in the Canadian Arctic Archipelago from C- and L-Band Synthetic Aperture  
624 Radar, *Can. J. Remote Sens.*, 45, 457–475, <https://doi.org/10.1080/07038992.2019.1647102>, 2019.

625 Campbell, K., Mundy, C. J., Landy, J. C., Delaforge, A., Michel, C., and Rysgaard, S.: Community dynamics of bottom-ice  
626 algae in Dease Strait of the Canadian Arctic, *Prog. Oceanogr.*, 149, 27–39, <https://doi.org/10.1016/j.pocean.2016.10.005>, 2016.

627 De Rijke-Thomas, C., Landy, J. C., Mallett, R., Willatt, R. C., Tsamados, M., and King, J.: Airborne Investigation of Quasi-  
628 Specular Ku-Band Radar Scattering for Satellite Altimetry Over Snow-Covered Arctic Sea Ice, *IEEE Trans. Geosci. Remote  
629 Sens.*, 61, 1–19, <https://doi.org/10.1109/TGRS.2023.3318263>, 2023.

630 Diaz, A., Ehn, J. K., Landy, J. C., Else, B. G. T., Campbell, K., and Papakyriakou, T. N.: The Energetics of Extensive Meltwater  
631 Flooding of Level Arctic Sea Ice, *J. Geophys. Res. Oceans*, 123, 8730–8748, <https://doi.org/10.1029/2018JC014045>, 2018.

632 Eicken, H., Grenfell, T. C., Perovich, D. K., Richter-Menge, J. A., and Frey, K.: Hydraulic controls of summer Arctic pack ice  
633 albedo, *Journal of Geophysical Research: Oceans*, 109, <https://doi.org/10.1029/2003JC001989>, 2004.

634 ESA: CryoSat-2 Product Handbook, 2013.

635 ESA: About CRYO2ICE - Earth Online:<https://earth.esa.int/eogateway/missions/cryosat/Cryo2Ice>, last access: 20 October  
636 2023, 2020.

637 Farrell, S., Duncan, K., Yi, D., Hendricks, S., Ricker, R., Buckley, E., and Baney, O.: Optimizing Dual-Band Satellite  
638 Altimetry to Map Declining Arctic Sea Ice, 2021, C31B-05, 2021.

639 Fons, S. W., Kurtz, N. T., Bagnardi, M., Petty, A. A., and Tilling, R. L.: Assessing CryoSat-2 Antarctic Snow Freeboard  
640 Retrievals Using Data From ICESat-2, *Earth Space Sci.*, 8, e2021EA001728, <https://doi.org/10.1029/2021EA001728>, 2021.

641 **Fredensborg Hansen, R. M., Skourup, H., Rinne, E., Høyland, K. V., Landy, J. C., Merkouriadi, I., and Forsberg, R.: Arctic  
642 Freeboard and Snow Depth From Near-Coincident CryoSat-2 and ICESat-2 (CRYO2ICE) Observations: A First Examination  
643 of Winter Sea Ice During 2020–2022, *Earth Space Sci.*, 11, e2023EA003313, <https://doi.org/10.1029/2023EA003313>, 2024.**

644 Galley, R. J., Else, B. G. T., Howell, S. E. L., Lukovich, J. V., And Barber, D. G.: Landfast Sea Ice Conditions in the Canadian  
645 Arctic: 1983-2009, *Arctic*, 65, 133–144, 2012.

646 Howell, S. E. L., Laliberté, F., Kwok, R., Derksen, C., and King, J.: Landfast ice thickness in the Canadian Arctic Archipelago  
647 from observations and models, *The Cryosphere*, 10, 1463–1475, <https://doi.org/10.5194/tc-10-1463-2016>, 2016.

648 Kacimi, S. and Kwok, R.: The Antarctic sea ice cover from ICESat-2 and CryoSat-2: freeboard, snow depth, and ice thickness,  
649 *The Cryosphere*, 14, 4453–4474, <https://doi.org/10.5194/tc-14-4453-2020>, 2020.

650 Kern, S., Khvorostovsky, K., Skourup, H., Rinne, E., Parsakhoo, Z. S., Djepa, V., Wadhams, P., and Sandven, S.: The impact  
651 of snow depth, snow density and ice density on sea ice thickness retrieval from satellite radar altimetry: results from the ESA-  
652 CCI Sea Ice ECV Project Round Robin Exercise, *The Cryosphere*, 9, 37–52, <https://doi.org/10.5194/tc-9-37-2015>, 2015.

653 Kurtz, N. T. and Farrell, S. L.: Large-scale surveys of snow depth on Arctic sea ice from Operation IceBridge, *Geophysical*  
654 *Research Letters*, 38, <https://doi.org/10.1029/2011GL049216>, 2011.

655 Kwok, R. and Markus, T.: Potential basin-scale estimates of Arctic snow depth with sea ice freeboards from CryoSat-2 and  
656 ICESat-2: An exploratory analysis, *Advances in Space Research*, 62, 1243–1250, <https://doi.org/10.1016/j.asr.2017.09.007>,  
657 2018.

658 Kwok, R., Cunningham, G., Hancock, D., Ivanoff, A., and Wimert, J.: Algorithm Theoretical Basis Document (ATBD) For  
659 Sea Ice Products, 2018.

660 Kwok, R., Kacimi, S., Markus, T., Kurtz, N. T., Studinger, M., Sonntag, J. G., Manizade, S. S., Boisvert, L. N., and Harbeck,  
661 J. P.: ICESat-2 Surface Height and Sea Ice Freeboard Assessed With ATM Lidar Acquisitions From Operation IceBridge,  
662 *Geophysical Research Letters*, 46, 11228–11236, <https://doi.org/10.1029/2019GL084976>, 2019.

663 Kwok, R., Bagnardi, M., Petty, A., and Kurtz, N.: ICESat-2 sea ice ancillary data - Mean Sea Surface Height Grids,  
664 <https://doi.org/10.5281/zenodo.4294048>, 2020.

665 Kwok, R., Petty, A. A., Bagnardi, M., Kurtz, N. T., Cunningham, G. F., Ivanoff, A., and Kacimi, S.: Refining the sea surface  
666 identification approach for determining freeboards in the ICESat-2 sea ice products, *The Cryosphere*, 15, 821–833,  
667 <https://doi.org/10.5194/tc-15-821-2021>, 2021.

668 Kwok, R., Petty, A., Bagnardi, M., Wimert, J. T., Cunningham, G. F., Hancock, D. W., Ivanoff, A., and Kurtz, N.: Ice, Cloud,  
669 and Land Elevation Satellite (ICESat-2) Project Algorithm Theoretical Basis Document (ATBD) for Sea Ice Products, version  
670 6, <https://doi.org/10.5067/9VT7NJWOTV3I>, 2023.

671 Lam, H-M., Geldsetzer, T., Howell, S.E.L., and Yackel, J. Snow Depth on Sea Ice and on Land in the Canadian Arctic from  
672 Long-Term Observations, *Atmosphere-Ocean*, 61:4, 217-233, <https://doi.org/10.1080/07055900.2022.2060178>, 2023.

673 Landy, J. C., Petty, A. A., Tsamados, M., and Stroeve, J. C.: Sea Ice Roughness Overlooked as a Key Source of Uncertainty  
674 in CryoSat-2 Ice Freeboard Retrievals, *Journal of Geophysical Research: Oceans*, 125, e2019JC015820,  
675 <https://doi.org/10.1029/2019JC015820>, 2020.

676 Laxon, S. W., Giles, K. A., Ridout, A. L., Wingham, D. J., Willatt, R., Cullen, R., Kwok, R., Schweiger, A., Zhang, J., Haas,  
677 C., Hendricks, S., Krishfield, R., Kurtz, N., Farrell, S., and Davidson, M.: CryoSat-2 estimates of Arctic sea ice thickness and  
678 volume, *Geophysical Research Letters*, 40, 732–737, <https://doi.org/10.1002/grl.50193>, 2013.

679 Leuschen, C. J., Swift, R. N., Comiso, J. C., Raney, R. K., Chapman, R. D., Krabill, W. B., and Sonntag, J. G.: Combination  
680 of laser and radar altimeter height measurements to estimate snow depth during the 2004 Antarctic AMSR-E Sea Ice field  
681 campaign, *Journal of Geophysical Research: Oceans*, 113, <https://doi.org/10.1029/2007JC004285>, 2008.

682 Magruder, L. A., Brunt, K. M., and Alonzo, M.: Early ICESat-2 on-orbit Geolocation Validation Using Ground-Based Corner  
683 Cube Retro-Reflectors, *Remote Sensing*, 12, 3653, <https://doi.org/10.3390/rs12213653>, 2020.

684 Mahoney, A., Gearheard, S., Oshima, T., and Qillaq, T.: Sea Ice Thickness Measurements from a Community-Based  
685 Observing Network, *Bulletin of the American Meteorological Society*, 90, 370–378,  
686 <https://doi.org/10.1175/2008BAMS2696.1>, 2009.

687 Maykut, G. A. and Untersteiner, N.: Some results from a time-dependent thermodynamic model of sea ice, *Journal of*  
688 *Geophysical Research* (1896-1977), 76, 1550–1575, <https://doi.org/10.1029/JC076i006p01550>, 1971.

689 Meier, W. and Stroeve, J.: An Updated Assessment of the Changing Arctic Sea Ice Cover, *Oceanog*,  
690 <https://doi.org/10.5670/oceanog.2022.114>, 2022.

691 Melling, H.: Sea ice of the northern Canadian Arctic Archipelago, *Journal of Geophysical Research: Oceans*, 107, 2-1-2–21,  
692 <https://doi.org/10.1029/2001JC001102>, 2002.

693 [Moran, P.A.P.: The interpretation of statistical maps, \*Journal of the Royal Statistical Society\*, 10, 243-251.](#)

694 Mundy, C. J., Barber, D. G., and Michel, C.: Variability of snow and ice thermal, physical and optical properties pertinent to  
695 sea ice algae biomass during spring, *Journal of Marine Systems*, 58, 107–120, <https://doi.org/10.1016/j.jmarsys.2005.07.003>,  
696 2005.

697 Moon, W., Nandan, V., Scharien, R. K., Wilkinson, J., Yackel, J. J., Barrett, A., Lawrence, I., Segal, R. A., Stroeve, J.,  
698 Mahmud, M., Duke, P. J., and Else, B.: Physical length scales of wind-blown snow redistribution and accumulation on  
699 relatively smooth Arctic first-year sea ice, *Environ. Res. Lett.*, 14, 104003, <https://doi.org/10.1088/1748-9326/ab3b8d>, 2019.

700 Nandan, V., Geldsetzer, T., Yackel, J., Mahmud, M., Scharien, R., Howell, S., King, J., Ricker, R., and Else, B.: Effect of  
701 Snow Salinity on CryoSat-2 Arctic First-Year Sea Ice Freeboard Measurements, *Geophysical Research Letters*, 44, 10,419-  
702 10,426, <https://doi.org/10.1002/2017GL074506>, 2017.

703 Nandan, V., Scharien, R. K., Geldsetzer, T., Kwok, R., Yackel, J. J., Mahmud, M. S., Rösel, A., Tonboe, R., Granskog, M.,  
704 Willatt, R., Stroeve, J., Nomura, D., and Frey, M.: Snow Property Controls on Modeled Ku-Band Altimeter Estimates of First-  
705 Year Sea Ice Thickness: Case Studies From the Canadian and Norwegian Arctic, *IEEE Journal of Selected Topics in Applied*  
706 *Earth Observations and Remote Sensing*, 13, 1082–1096, <https://doi.org/10.1109/JSTARS.2020.2966432>, 2020.

707 Neumann, T. A., Martino, A. J., Markus, T., Bae, S., Bock, M. R., Brenner, A. C., Brunt, K. M., Cavanaugh, J., Fernandes, S.  
708 T., Hancock, D. W., Harbeck, K., Lee, J., Kurtz, N. T., Luers, P. J., Luthcke, S. B., Magruder, L., Pennington, T. A., Ramos-  
709 Izquierdo, L., Rebold, T., Skoog, J., and Thomas, T. C.: The Ice, Cloud, and Land Elevation Satellite – 2 mission: A global  
710 geolocated photon product derived from the Advanced Topographic Laser Altimeter System, *Remote Sensing of Environment*,  
711 233, 111325, <https://doi.org/10.1016/j.rse.2019.111325>, 2019.

712 Raney, R. K. and Leuschen, C.: Technical Support for the Deployment Of Radar and Laser Altimeters during LaRA 2002,  
713 Final Report, 21, 2003.

714 Ricker, R., Hendricks, S., Helm, V., Skourup, H., and Davidson, M.: Sensitivity of CryoSat-2 Arctic sea-ice freeboard and  
715 thickness on radar-waveform interpretation, *The Cryosphere*, 8, 1607–1622, <https://doi.org/10.5194/tc-8-1607-2014>, 2014.

716 Ricker, R., Fons, S., Jutila, A., Hutter, N., Duncan, K., Farrell, S. L., Kurtz, N. T., and Fredensborg Hansen, R. M.: Linking  
717 scales of sea ice surface topography: evaluation of ICESat-2 measurements with coincident helicopter laser scanning during  
718 MOSAiC, *The Cryosphere*, 17, 1411–1429, <https://doi.org/10.5194/tc-17-1411-2023>, 2023.

719 Rotermund, L. M., Williams, W. J., Klymak, J. M., Wu, Y., Scharien, R. K., and Haas, C.: The Effect of Sea Ice on Tidal  
720 Propagation in the Kitikmeot Sea, Canadian Arctic Archipelago, *Journal of Geophysical Research: Oceans*, 126,  
721 e2020JC016786, <https://doi.org/10.1029/2020JC016786>, 2021.

722 Tilling, R. L., Ridout, A., and Shepherd, A.: Estimating Arctic sea ice thickness and volume using CryoSat-2 radar altimeter  
723 data, *Advances in Space Research*, 62, 1203–1225, <https://doi.org/10.1016/j.asr.2017.10.051>, 2018.

724 Ullaby, F. T., Moore, R. K., and Fung, A. K.: Microwave Remote Sensing. Active and Passive., *Geological Magazine*, 124,  
725 88–88, <https://doi.org/10.1017/S0016756800015831>, 1987.

726 Warren, S. G., Rigor, I. G., Untersteiner, N., Radionov, V. F., Bryazgin, N. N., Aleksandrov, Y. I., and Colony, R.: Snow  
727 Depth on Arctic Sea Ice, *Journal of Climate*, 12, 1814–1829, [https://doi.org/10.1175/1520-0442\(1999\)012<1814:SDOASI>2.0.CO;2](https://doi.org/10.1175/1520-0442(1999)012<1814:SDOASI>2.0.CO;2), 1999.

729 Webster, M., Gerland, S., Holland, M., Hunke, E., Kwok, R., Lecomte, O., Massom, R., Perovich, D., and Sturm, M.: Snow  
730 in the changing sea-ice systems, *Nature Clim Change*, 8, 946–953, <https://doi.org/10.1038/s41558-018-0286-7>, 2018.

731 Webster, M. A., Rigor, I. G., Nghiem, S. V., Kurtz, N. T., Farrell, S. L., Perovich, D. K., and Sturm, M.: Interdecadal changes  
732 in snow depth on Arctic sea ice, *Journal of Geophysical Research: Oceans*, 119, 5395–5406,  
733 <https://doi.org/10.1002/2014JC009985>, 2014a.

734 Willatt, R., Laxon, S., Giles, K., Cullen, R., Haas, C., and Helm, V.: Ku-band radar penetration into snow cover on Arctic sea  
735 ice using airborne data, *Ann. Glaciol.*, 52, 197–205, <https://doi.org/10.3189/172756411795931589>, 2011.

736 Xu, C., Mikhael, W., Myers, P. G., Else, B., Sims, R. P., and Zhou, Q.: Effects of Seasonal Ice Coverage on the Physical  
737 Oceanographic Conditions of the Kitikmeot Sea in the Canadian Arctic Archipelago, *Atmosphere-Ocean*, 59, 214–232,  
738 <https://doi.org/10.1080/07055900.2021.1965531>, 2021.

739 Yackel, J., Geldsetzer, T., Mahmud, M., Nandan, V., Howell, S. E. L., Scharien, R. K., and Lam, H. M.: Snow Thickness  
740 Estimation on First-Year Sea Ice from Late Winter Spaceborne Scatterometer Backscatter Variance, *Remote Sens.*, 11, 417,  
741 <https://doi.org/10.3390/rs11040417>, 2019.

742 Zheng, J., Geldsetzer, T., and Yackel, J.: Snow thickness estimation on first-year sea ice using microwave and optical remote  
743 sensing with melt modelling, *Remote Sens. Environ.*, 199, 321–332, <https://doi.org/10.1016/j.rse.2017.06.038>, 2017.

744

745

746 **Appendix A**

747 **Table A1: Geophysical corrections applied on the IS2 ATL07 product. The range represents the typical variation in the corrections**  
 748 **as reported in the IS2 Algorithm Theoretical Basis Document (ATBD).**

<b>Geophysical Correction</b>	<b>Typical Range</b>	<b>Source</b>
Solid Earth Tide	-19 to +27 cm	IERS 2010 (Applied in ATL03)
Solid Earth Pole Tides	-0.6 to +0.7 cm	IERS 2010 (Applied on ATL03)
Ocean Pole tides	+/- 2 mm	IERS 2010 (Applied in ATL03)
Ocean loading	-9.7 to +9.3 cm	GOT4.8 Ocean Tide Model (Applied in ATL07)
Ocean Tides	-6.2 to +6.2 m	GOT4.8 Ocean Tide Model (Applied in ATL07)
Long period equilibrium tides	-7.1 to +6.0 cm	GOT4.8 Ocean Tide Model (Applied in ATL07)
Inverted barometer	-53 to +94 cm	ATL09/GEOS5 FP-IT (Applied in ATL07)

749

750 **Appendix B**

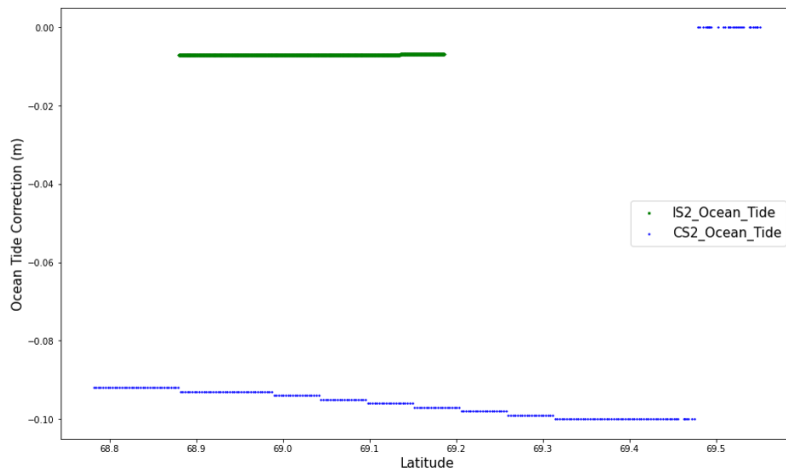
751 **Table B1: Geophysical Corrections applied in the CS2 Level 2 product. The typical range values are reported in the Cryosat-2**  
 752 **Baseline E Level 2 Product Handbook.**  
 753

<b>Geophysical Correction</b>	<b>Typical Range</b>	<b>Source</b>
Ocean Tide	-50 to +50 cm	Finite Element Solution FES 2004 Tide Model
Long-Period Equilibrium Ocean Tide	< 1cm	Finite Element Solution FES 2004 Tide Model
Ocean Loading	-2 to +2 cm	Finite Element Solution FES 2004 Tide Model
Solid Earth Tide	-30 to +30 cm	Cartwright Tide model (Cartwright & Edden, 1973)
Geocentric Polar Tide	-2 to +2 cm	Historical Pole Positions from CNES
Inverted Barometer	-15 to +15 cm	Dynamic Surface Pressure from Meteo France

754  
755 **Appendix C**

756  
757





758

759 **Figure C1: Ocean tidal correction used in the IS2 and CS2 tracks. The IS2 ocean tide corrections are shown in green while the CS2**  
 760 **ocean tide corrections are shown in blue.**

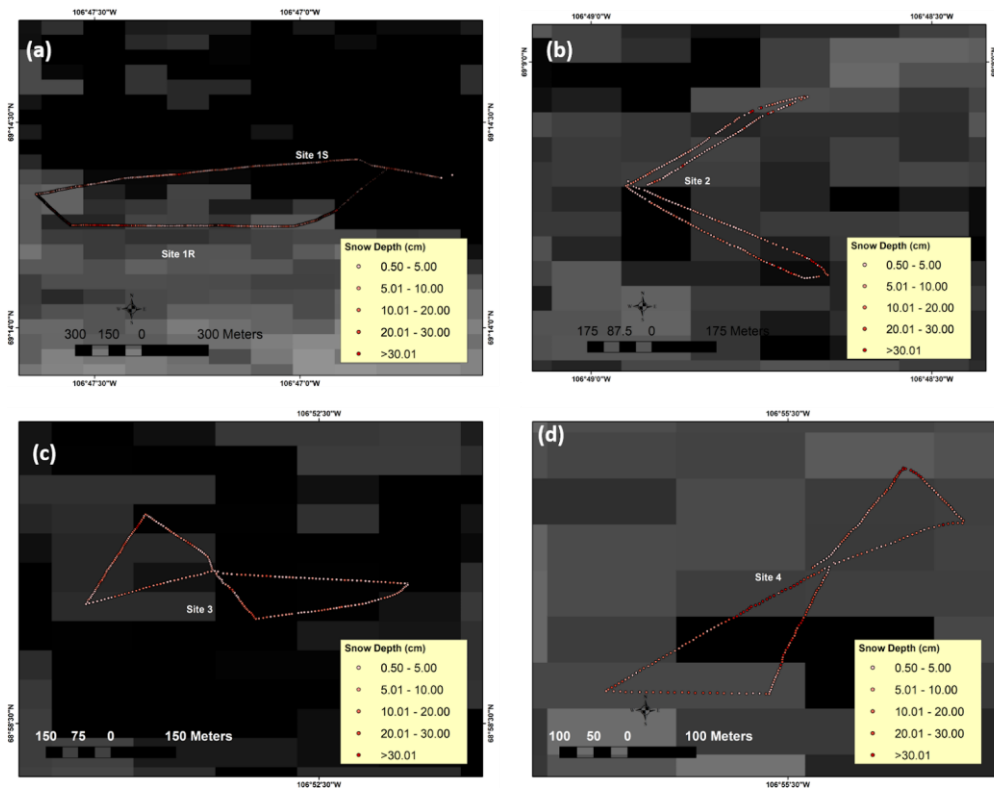
761 **Appendix D**

762 ▲

**Formatted:** Font: Bold

**Formatted:** Font: 10 pt, Not Bold, Font color: Auto

**Formatted:** Space After: 0 pt, Line spacing: 1.5 lines



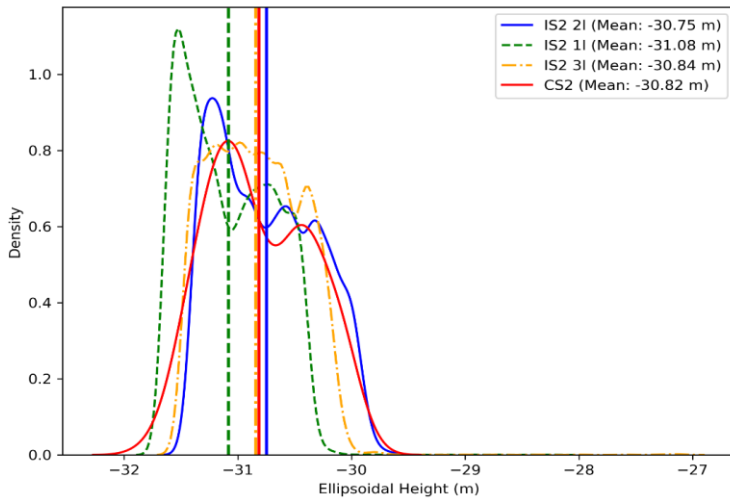
763  
764  
765 Figure D1: The in-situ snow depth transects conducted in (a) Site 1 (b) Site 2 (c) Site 3 and (d) Site 4. The spatial  
766 distribution of the snow depths are included for each site.

774

775

**Appendix E**

**Formatted:** Font: 10 pt, Bold



776

777

Figure E1: ATL07 ICESat-2 strong beam (IS2 1I, 2I, 3I) sea ice height ellipsoidal height distributions compared to the CS2 height ellipsoidal height distribution.

778

779

780

781

782

783

784

785

786

787

788

789

790

791 **Appendix F**

792 **Table F1 In-situ versus Cryo2Ice snow depth distribution statistics retrieved using 300 meter averaged IS2 and CS2 height**

		<b>Mean (cm)</b>	<b>Median (cm)</b>	<b>Lower Quartile (cm)</b>	<b>Upper Quartile (cm)</b>	<b>Inter-quartile range (cm)</b>
Site 1	In-Situ	12.2	7.8	4.1	16.3	12.2
	Cryo2Ice	4.7	4.9	-1.8	9.8	11.6
Site 2	In-Situ	9.7	5.2	3.7	9.2	5.5
	Cryo2Ice	1.9	4.8	-5.9	8.5	14.4
Site 3	In-Situ	8.9	6.9	4.2	11.9	7.7
	Cryo2Ice	0.61	3.4	-5.4	5.8	11.2
Site 4	In-Situ	17.1	13.8	6.7	22.4	15.7
	Cryo2Ice	10.6	8.3	-0.6	18.5	19.1

793  
794  
795  
796  
797  
798  
799  
800  
801  
802  
803

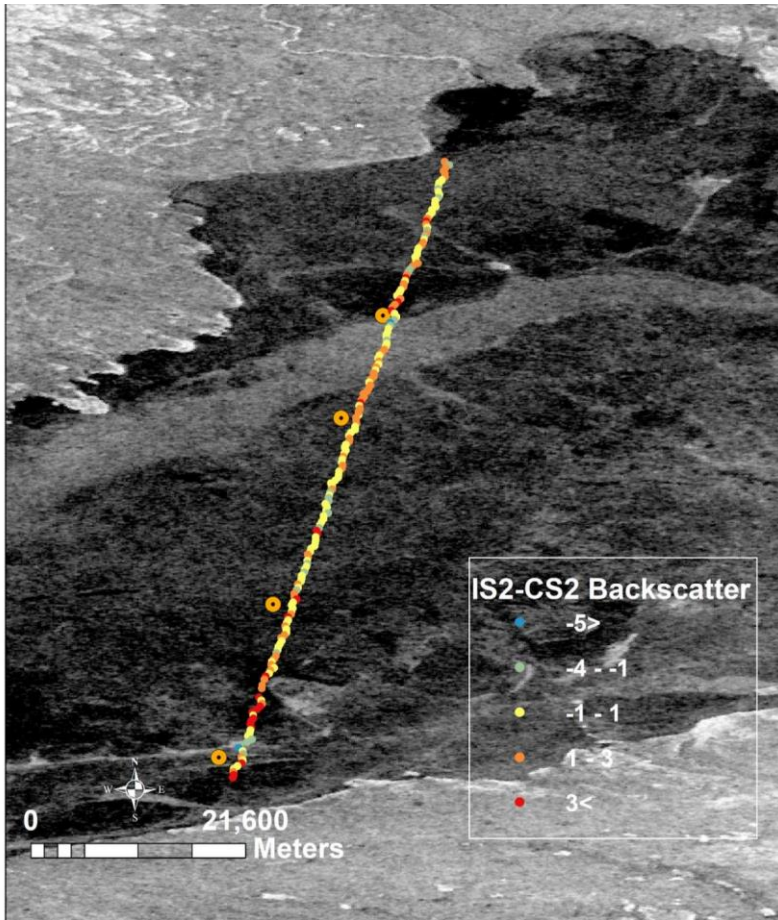
**Table F2 In-situ versus Cryo2Ice snow depth distribution statistics retrieved using 1-km averaged IS2 and CS2 height**

		<b>Mean (cm)</b>	<b>Median (cm)</b>	<b>Lower Quartile (cm)</b>	<b>Upper Quartile (cm)</b>	<b>Inter-quartile range (cm)</b>
	In-Situ	12.2	7.8	4.1	16.3	12.2

Site 1	Cryo2Ice	7.1	6.3	4.6	8.8	4.2
Site 2	In-Situ	9.7	5.2	3.7	9.2	5.5
	Cryo2Ice	4.0	4.9	-8.4	8.2	16.6
Site 3	In-Situ	8.9	6.9	4.2	11.9	7.7
	Cryo2Ice	6.5	2.3	-1.7	3.8	5.5
Site 4	In-Situ	17.1	13.8	6.7	22.4	15.7
	Cryo2Ice	18.7	8.3	15.1	24.2	9.1

804

805 **Appendix G**



806

807 Figure G1 Spatial Distribution of the backscatter between IS2 and CS2 retrieved from collocated Sentinel-1 image from 5<sup>th</sup>

808 May 2022

809